

# Using Subsystem $M_{T2}$ for Complete Mass Determinations in Decay Chains with Missing Energy at Hadron Colliders

---

**Michael Burns**

*Physics Department, University of Florida, Gainesville, FL 32611, USA*

**Kyoungchul Kong**

*Theoretical Physics Department, Fermilab, Batavia, IL 60510, USA*

**Konstantin T. Matchev, Myeonghun Park**

*Physics Department, University of Florida, Gainesville, FL 32611, USA*

ABSTRACT: We propose to use the  $M_{T2}$  concept to measure the masses of *all* particles in SUSY-like events with two unobservable, identical particles. To this end we generalize the usual notion of  $M_{T2}$  and define a new  $M_{T2}^{(n,p,c)}$  variable, which can be applied to various subsystem topologies, as well as the full event topology. We derive analytic formulas for its endpoint  $M_{T2,max}^{(n,p,c)}$  as a function of the unknown test mass  $\tilde{M}_c$  of the final particle in the subchain and the transverse momentum  $p_T$  due to radiation from the initial state. We show that the endpoint functions  $M_{T2,max}^{(n,p,c)}(\tilde{M}_c, p_T)$  may exhibit three different types of kinks and discuss the origin of each type. We prove that the subsystem  $M_{T2}^{(n,p,c)}$  variables by themselves already yield a sufficient number of measurements for a *complete* determination of the mass spectrum (including the overall mass scale). As an illustration, we consider the simple case of a decay chain with up to three heavy particles,  $X_2 \rightarrow X_1 \rightarrow X_0$ , which is rather problematic for all other mass measurement methods. We propose three different  $M_{T2}$ -based methods, each of which allows a complete determination of the masses of particles  $X_0$ ,  $X_1$  and  $X_2$ . The first method only uses  $M_{T2}^{(n,p,c)}$  endpoint measurements at a single fixed value of the test mass  $\tilde{M}_c$ . In the second method the unknown mass spectrum is fitted to one or more endpoint functions  $M_{T2,max}^{(n,p,c)}(\tilde{M}_c, p_T)$  exhibiting a kink. The third method is hybrid, combining  $M_{T2}$  endpoints with measurements of kinematic edges in invariant mass distributions. As a practical application of our methods, we show that the dilepton  $W^+W^-$  and  $t\bar{t}$  samples at the Tevatron can be used for an independent determination of the masses of the top quark, the  $W$  boson and the neutrino, without any prior assumptions.

KEYWORDS: Hadronic Colliders, Beyond Standard Model, Supersymmetry Phenomenology,  
Large Extra Dimensions.

---

## Contents

<b>1. Introduction</b>	<b>1</b>
<b>2. Mass measurement methods in missing energy events</b>	<b>4</b>
2.1 Endpoint method	5
2.2 Polynomial method	6
2.3 $M_{T2}$ method	10
<b>3. Defining a subsystem <math>M_{T2}</math> variable</b>	<b>10</b>
<b>4. A short decay chain <math>X_2 \rightarrow X_1 \rightarrow X_0</math></b>	<b>13</b>
4.1 The subsystem variable $M_{T2}^{(1,1,0)}$	14
4.2 The subsystem variable $M_{T2}^{(2,2,1)}$	20
4.3 The subsystem variable $M_{T2}^{(2,2,0)}$	22
4.4 The subsystem variable $M_{T2}^{(2,1,0)}$	27
<b>5. <math>M_{T2}</math>-based mass measurement methods</b>	<b>29</b>
5.1 Pure $M_{T2}$ endpoint method	31
5.2 $M_{T2}$ endpoint shapes and kinks	32
5.3 Hybrid method: $M_{T2}$ endpoints plus an invariant mass endpoint	34
<b>6. Summary and conclusions</b>	<b>36</b>
<b>A. Appendix: Analytical expressions for <math>M_{T2,max}^{(n,p,c)}(\tilde{M}_c, p_T)</math></b>	<b>39</b>
A.1 The subsystem variable $M_{T2,max}^{(n,n,n-1)}(\tilde{M}_{n-1}, p_T)$	40
A.2 The subsystem variable $M_{T2,max}^{(n,n,n-2)}(\tilde{M}_{n-2}, p_T)$	40
A.3 The subsystem variable $M_{T2,max}^{(n,n-1,n-2)}(\tilde{M}_{n-2}, p_T)$	42

---

## 1. Introduction

The ongoing Run II of the Fermilab Tevatron and the now commencing run of the Large Hadron Collider (LHC) at CERN are on the hunt for new physics beyond the Standard Model (BSM) at the TeV scale. Arguably the most compelling *phenomenological* evidence for BSM particles and interactions at the TeV scale is provided by the dark matter problem [1], whose solution requires new particles and interactions BSM. A typical particle dark matter candidate does not interact in the detector and can only manifest itself as missing energy.

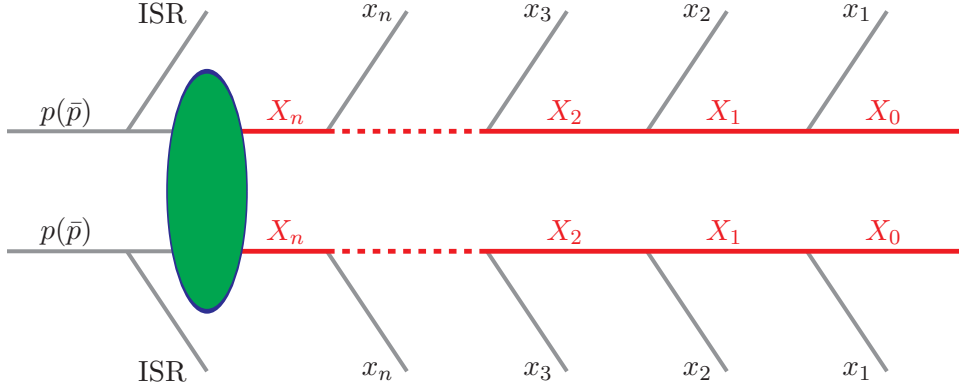


**Figure 1:** The generic event topology under consideration in this paper. The particles  $X_i$ ,  $1 \leq i \leq n$ , are new BSM particles which appear as promptly decaying, on-shell intermediate resonances. The particles  $x_i$  are the corresponding SM decay products, which are all visible in the detector, i.e. we assume that there are no neutrinos among them. ISR stands for generic initial state radiation with total transverse momentum  $\vec{p}_T$ .  $X_0$  is a BSM particle which is invisible in the detector. The integer  $n$  counts the total number of *intermediate* BSM particles in each chain, so that the *total* number of BSM particles in each chain is  $n + 1$ . For simplicity, in this paper we shall only consider symmetric events, in which the two decay chains are identical. The generalization of our methods to asymmetric decay chains is straightforward.

The dark matter problem therefore greatly motivates the study of missing energy signatures at the Tevatron and the LHC [2].

The long lifetime of the dark matter particle is typically ensured by some new exact symmetry<sup>1</sup>, under which the SM particles are neutral, while the BSM particles are charged. This setup implies that the new particles will be pair-produced, and each of the two cascades will terminate in the dark matter candidate, giving rise to missing energy in the detector. (A generic example of this topology is shown in Fig. 1.) Since the energies and momenta of the final two invisible particles  $X_0$  are not measured, one cannot directly apply resonance mass reconstruction techniques<sup>2</sup>. This represents a significant challenge for determining the masses  $M_i$  of the new particles  $X_i$ . In recognition of this problem, there has been a recent resurgence of interest in the development of different methods for mass measurements in cascade decays with missing energy [12–48]. Most of these techniques fall into one of the following three categories:

- **I. Endpoint methods.** They rely on the kinematic endpoints [12, 14–16, 20, 21, 25] or shapes [22, 23, 46] of various invariant mass distributions constructed out of the visible (SM) decay products  $x_i$  in the cascade chain.
- **II. Polynomial methods.** Here one attempts exact event reconstruction using the measured momenta of the SM particles and the measured missing transverse momentum

<sup>1</sup>Some well known examples are:  $R$ -parity in supersymmetry [3], KK parity in models with extra dimensions [4–7],  $T$ -parity in Little Higgs models [8, 9],  $U$ -parity [10, 11] etc.

<sup>2</sup>See, however, Section 2.2.

[18, 19, 27, 38, 39].

- **III.  $M_{T2}$  methods.** These methods explore the transverse invariant mass variable  $M_{T2}$  originally proposed in [13] and later used and developed in [17, 24, 26, 28, 37, 40, 41, 45]. Recently it was shown that under certain circumstances, the endpoint of the  $M_{T2}$  distribution, when considered as a function of the unknown test mass  $\tilde{M}_0$  of the lightest new particle  $X_0$ , exhibits a kink and the true mass  $M_0$  of  $X_0$ , i.e. at  $\tilde{M}_0 = M_0$  [29–32, 36].

One could also combine two or more of these techniques into a hybrid method, e.g. a mixed polynomial and endpoint method [34], a mixed  $M_{T2}$  and endpoint method [33, 43], or a mixed  $M_{T2}$  and polynomial method [47, 48]. In Section 2 we shall describe in detail each of these three basic approaches **I** - **III**. We shall then contrast them to each other and discuss their pros and cons. In particular, we shall concentrate on their applicability as a function of the length of the decay chain, i.e. the number  $n$  of intermediate resonances in Fig. 1. We shall find that for sufficiently long decay chains, namely  $n \geq 3$ , each method **I** - **III** *by itself* is able to completely determine the unknown particle spectrum, at least as a matter of principle. Therefore, if Nature is so kind to us as to present us with such a long decay chain, it does not really matter which of the three methods above we decide to use – sooner or later, success will be guaranteed with each one.

However, if the decay chain happens to be relatively short, i.e.  $n \leq 2$ , neither method **I**, nor method **II**, nor a hybrid combination of **I** and **II** will be able to completely determine the unknown particle mass spectrum. In contrast, method **III** *by itself* can still provide a sufficient number of measurements for a *complete* determination of the mass spectrum of the new particles. We argue that in order to achieve this, the conventional  $M_{T2}$  variable needs to be promoted to a more general quantity  $M_{T2}^{(n,p,c)}$ , which can be applied not only to the whole event, but also to a particular sub-chain starting at  $X_p$  and ending in  $X_c$  [41, 45]. We present the basic steps for this generalization in Section 3, where we also introduce our conventions and notation. Then in Section 4 we concentrate on the problematic case of  $n \leq 2$  and discuss what type of  $M_{T2}^{(n,p,c)}$  measurements are available in that case. We then show that the newly defined  $M_{T2}^{(n,p,c)}$  may also exhibit a kink in the graph of its endpoint  $M_{T2,max}^{(n,p,c)}$  as a function of the test mass  $\tilde{M}_c$ . In order to be able to properly interpret this kink, we derive analytic expressions for the function  $M_{T2,max}^{(n,p,c)}(\tilde{M}_c, p_T)$ , including the effect of initial state radiation (ISR) with some arbitrary transverse momentum  $p_T$  (see Fig. 1). In all cases, a kink would always appear at  $\tilde{M}_c = M_c$ :

$$\left( \frac{\partial M_{T2,max}^{(n,p,c)}(\tilde{M}_c, p_T)}{\partial \tilde{M}_c} \right)_{\tilde{M}_c=M_c-\epsilon} \neq \left( \frac{\partial M_{T2,max}^{(n,p,c)}(\tilde{M}_c, p_T)}{\partial \tilde{M}_c} \right)_{\tilde{M}_c=M_c+\epsilon}, \quad (1.1)$$

and the value of  $M_{T2,max}^{(n,p,c)}$  at that point reveals the true mass  $M_p$  of the mother particle  $X_p$ :

$$M_{T2,max}^{(n,p,c)}(M_c, p_T) = M_p. \quad (1.2)$$

However, there may be up to three different reasons for the origin of the kink (1.1). For example, in the case of  $M_{T2,max}^{(1,1,0)}(\tilde{M}_0, p_T)$  and  $M_{T2,max}^{(2,2,1)}(\tilde{M}_1, p_T)$  with non-zero  $p_T$ , the kink

arises due to recoils against the ISR jets, as explained in [30, 31] (see Sections 4.1 and 4.2 below). On the other hand, in the case of  $M_{T2,max}^{(2,2,0)}(\tilde{M}_0, p_T = 0)$ , the kink is due to the variable mass of the composite system of SM particles  $\{x_1 x_2\}$ , as already observed in Refs. [29, 32] (see Section 4.3 below). Finally, for  $M_{T2,max}^{(2,1,0)}(\tilde{M}_0, p_T = 0)$ , we encounter a new type of kink, which arises due to the decay of a heavier particle (in this case  $X_2$ ) upstream (see Section 4.4).

In Section 5 we propose three different methods for measuring the masses of all the particles in the problematic case of an  $n = 2$  decay chain. With the first method, presented in Section 5.1, we always consider a fixed value of the test mass (for convenience we choose it to be zero), and perform a sufficient number of  $M_{T2}^{(n,p,c)}$  endpoint measurements for various  $n$ ,  $p$  and  $c$ . In our second method, described in Section 5.2, we choose a suitable  $M_{T2}^{(n,p,c)}$  variable whose endpoint  $M_{T2,max}^{(n,p,c)}$  exhibits a kink, and then fit for the function  $M_{T2,max}^{(n,p,c)}(\tilde{M}_c, p_T)$ . Our last method, presented in Section 5.3, is hybrid, in the sense that we use combined information from the measured endpoints of some  $M_{T2}$  distributions, as well as the measured endpoints of certain invariant mass distributions. Neither of our three methods relies on reconstructing the actual momentum of each missing particle.

All of our discussion throughout the paper will be completely model-independent and can be applied to any BSM scenario, including supersymmetry, extra dimensions, little Higgs theory etc. In Section 5, however, we shall use a specific example in order to illustrate each of our three proposed methods. Instead of considering a decay chain of some BSM model, we chose to select an example which is already present in the Tevatron data, and will soon be tested at the LHC as well: the dilepton event samples from top quark pair production and from  $W$ -pair production. Those two dilepton samples satisfy all of our assumptions, and would be a perfect testing ground for any new ideas about mass measurements in missing energy events from new physics. In Section 5 we will show that using any one of our three  $M_{T2}$ -based mass measurement methods, one can in principle determine the mass of each of the three particles: top quark,  $W$ -boson, and neutrino, independently and in a completely model-independent fashion. Section 6 contains a summary and a discussion of our main results. In Appendix A we collect all relevant formulas for the endpoint functions  $M_{T2,max}^{(n,p,c)}(\tilde{M}_c, p_T)$ .

## 2. Mass measurement methods in missing energy events

Let us now discuss in some detail each of the three basic methods **I** - **III** for mass measurements in missing energy events. The basic topology is shown in Fig. 1, where the particles  $X_i$ ,  $0 \leq i \leq n$ , (denoted in red) are new BSM particles, and the particles  $x_i$ ,  $1 \leq i \leq n$ , (denoted in black) are the corresponding SM decay products. ISR stands for generic initial state radiation with total transverse momentum  $\vec{p}_T$ .  $X_0$  is a dark matter candidate which is invisible in the detector. For simplicity, in this paper we shall make two assumptions, each of which can be easily relaxed without significantly changing our conclusions. First, we shall assume that the intermediate particles  $X_i$ ,  $1 \leq i \leq n$ , are all on-shell, i.e. their masses  $M_i \equiv M_{X_i}$  obey the hierarchy

$$M_n > M_{n-1} > \dots > M_1 > M_0 . \quad (2.1)$$

Consequently, all decays along our decay chain are two-body, i.e. each SM decay product  $x_i$  is a single particle of mass  $m_i \equiv m_{x_i}$ . In this paper we will also only concentrate on the commonly encountered case where  $x_i$  is either a lepton, photon or jet, i.e. massless:

$$m_i = 0, \quad i = 1, \dots, n . \quad (2.2)$$

Second, we shall also assume that our events are symmetric, i.e. the two decay chains are identical. Again, this assumption can be easily dropped and one could consider asymmetric events as well (see, for example, Ref. [45]). These assumptions are made only for simplicity. All of our subsequent discussion can be easily generalized to include off-shell decays, simply by promoting some of the visible SM particles  $x_i$  to composite particles with variable mass. For example, Appendix A already contains some results for an off-shell case, while the study of asymmetric events is postponed for future work [49].

We shall use the integer  $n$  to count the total number of *intermediate* on-shell BSM particles in each chain. Then, the total number of new BSM particles in the decay chain is  $n + 1$ . With those preliminaries, we are ready to discuss each of the three different methods for mass measurements in missing energy events.

## 2.1 Endpoint method

With this method, one forms the invariant mass distributions  $M_{x_{i_1} x_{i_2} \dots x_{i_k}}$  of various groups of  $k$  SM decay products  $x_i$ , where the number  $k$  in principle can range from 2 to  $n$ . Each such distribution exhibits an *upper* kinematic endpoint, which can be related to the underlying unknown masses  $M_i$ . If one makes a sufficient number of independent upper endpoint measurements, the system of equations giving the kinematic endpoints  $E_j$  in terms of the masses  $M_i$

$$E_j = E_j(M_0, \dots, M_n), \quad j = 0, \dots, n \quad (2.3)$$

can be solved for the masses  $M_i$ , although on some occasions the solution may not be unique – see, e.g. [50, 51].

Clearly, the method will be fully successful only if the number of measurements  $N_m$  is no less than the number of unknown parameters  $N_p$ . For the decay chain of Fig. 1, the number of unknown mass parameters  $N_p$  is simply the total number of BSM particles:

$$N_p = n + 1 . \quad (2.4)$$

How many measurements  $N_m$  are available with this method? The answer to this question depends on the length of the decay chain. It is easy to see that, if  $n = 1$ , there are no endpoint measurements at all; if  $n = 2$ , there is a single measurement of the endpoint of the  $M_{x_1 x_2}$  distribution, etc. In general, for an arbitrary fixed  $n$ , the number of different invariant mass distributions  $M_{x_{i_1} x_{i_2} \dots x_{i_k}}$  that one can form and study, is equal to the number of ways in which we can select a group of at least two objects from a set of  $n$  objects, and is given by

$$N_m = 2^n - (n + 1) . \quad (2.5)$$

Strictly speaking, eq. (2.5) only gives an upper bound on the number of independent *upper* endpoints in the invariant mass distributions. Indeed, there are certain cases where not all of the upper kinematic endpoints are independent. For example, consider the familiar case of a squark decay chain in supersymmetry:  $X_3 = \tilde{q}$ ,  $X_2 = \tilde{\chi}_2^0$ ,  $X_1 = \tilde{\ell}$  and  $X_0 = \tilde{\chi}_1^0$ . The SM decay products consist of a quark jet  $q$  and two leptons:  $\ell^+$  and  $\ell^-$ . It is well known that in some regions of parameter space the upper endpoint of the  $M_{q\ell\ell}$  distribution does not provide an independent measurement, since it can be related to the upper endpoints of the  $M_{\ell^+\ell^-}$  and  $M_{q\ell^{(high)}} \equiv \max\{M_{q\ell^+}, M_{q\ell^-}\}$  distributions [20]. Fortunately, one can use additional measurements from the *lower* endpoints of suitably restricted invariant mass distributions, e.g.  $M_{q\ell}(\theta > \frac{\pi}{2})$  [14]. We see that the precise count of the number of measurements  $N_m$  available in the endpoint method is somewhat model-dependent, but nevertheless, the estimate (2.5) is sufficient to make our main point below.

From eqs. (2.4) and (2.5) it readily follows that the number of undetermined parameters with this method is

$$N_p - N_m = 2(n + 1) - 2^n . \quad (2.6)$$

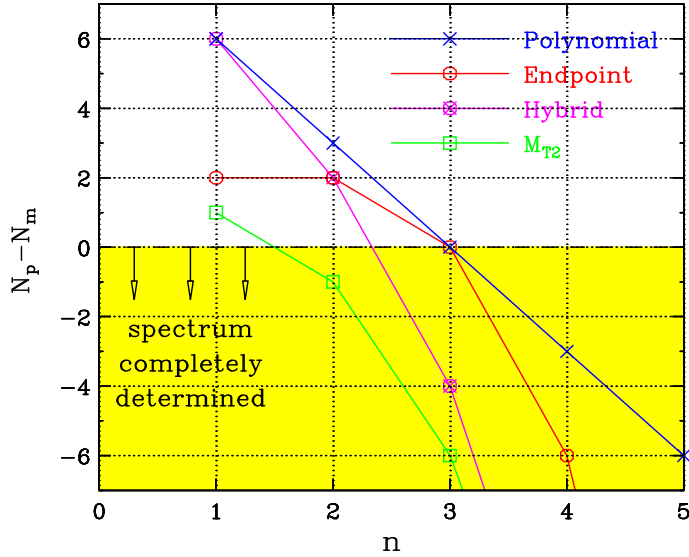
The dependence of this quantity on the length of the decay chain is plotted in Fig. 2 with red open circles, connected with red line segments. The yellow-shaded region in the figure is where  $N_m \geq N_p$ , so that we have a sufficient number of measurements for a *complete* determination of the heavy particle spectrum. Conversely, whenever a symbol appears inside the white region, where  $N_m < N_p$ , there is only partial information about the mass spectrum and the spectrum cannot be fully determined.

Fig. 2 reveals that the endpoint method cannot succeed unless  $n \geq 3$ . This conclusion has already been confirmed by numerous studies of various low-energy SUSY models, where one considers a decay chain of sufficient length:  $n = 3$  as in the squark example mentioned above, or  $n = 4$  as for a gluino chain [21]. On the other hand, if  $n = 1$  or  $n = 2$ , with this method we are unable to pin down *all* of the new particle masses, even as a matter of principle. These are exactly the cases where the additional information from mass measurements at future lepton colliders has been seen as extremely useful [52].

## 2.2 Polynomial method

The basic idea behind the method is to use all of the available experimental information in each event, and enforce a sufficient number of constraints, which would allow to actually solve for the unknown momenta of the missing particles  $X_0$ . Before we analyze this method in more detail, let us introduce some of our notations and conventions. We shall use lowercase letters to denote various quantities relating to the SM particles  $x_i$ ,  $1 \leq i \leq n$ . At the same time, we shall use a superscript  $(k)$  to denote whether a particular quantity belongs to the upper ( $k = 1$ ) or lower ( $k = 2$ ) decay chain in Fig. 1. For example, the 4-momentum of the SM particle  $x_i$  in the  $k$ -th chain will be denoted as  $p_i^{(k)}$ , the corresponding transverse momentum will be  $\vec{p}_{iT}^{(k)}$ , while the mass of  $x_i$  will simply be  $m_i$ . On the other hand, uppercase letters will denote quantities relating to the BSM particles  $X_i$ ,  $0 \leq i \leq n$ . Thus the 4-momentum of the BSM particle  $X_i$  appearing in the  $k$ -th chain is  $P_i^{(k)}$ , the corresponding transverse





**Figure 2:** The dependence of the number of undetermined parameters  $N_p - N_m$  as a function of the number  $n$  of intermediate heavy resonances in the decay chains of Fig. 1, for various mass determination methods:  $M_{T2}$  method (green, open squares), endpoint method (red, open circles), polynomial method for  $N_{ev} = 2$  (blue,  $\times$  symbols), or a hybrid method which is a combination of the latter two methods (magenta,  $\otimes$  symbols). Within the yellow-shaded region the number of unknowns  $N_p$  does not exceed the number of measurements  $N_m$  for the corresponding method, and the mass spectrum can be completely determined.

momentum is  $\vec{P}_{iT}^{(k)}$ , and the mass is  $M_i$ . One should keep in mind that for SM particles the index  $i$  runs from 1 to  $n$ , while for BSM particles  $i$  runs from 0 to  $n$ .

In order to apply the polynomial method, one uses the experimentally measured 4-momenta  $p_i^{(k)}$  as well as the missing transverse momentum  $\vec{p}_{T,miss}$  in the event. Then, one imposes the mass shell constraints for the intermediate BSM particles  $X_i$  and tries to solve the resulting system of equations for the 8 unknown components of the 4-momenta  $P_0^{(k)}$  of the missing particles  $X_0$ . Including the  $n + 1$  unknown masses  $M_i$ , this amounts to a total of

$$N_p = 8 + (n + 1) = n + 9 \quad (2.7)$$

unknown parameters. How many measurements (constraints) are present in this case? First, there is a total of  $2(n + 1)$  mass-shell conditions: one for each BSM particle  $X_i$  in each of the two decay chains in Fig. 1

$$M_i^2 = \left(P_i^{(1)}\right)^2 = \left(P_i^{(2)}\right)^2, \quad i = 0, 1, \dots, n. \quad (2.8)$$

Using energy and momentum conservation

$$P_i^{(k)} = P_0^{(k)} + \sum_{j=1}^i p_j^{(k)}, \quad k = 1, 2, \quad (2.9)$$

these constraints can be rewritten in terms of the unknown variables  $P_0^{(k)}$ :

$$M_i^2 = \left( P_0^{(1)} + \sum_{j=1}^i p_j^{(1)} \right)^2 = \left( P_0^{(2)} + \sum_{j=1}^i p_j^{(2)} \right)^2, \quad i = 0, 1, \dots, n. \quad (2.10)$$

Furthermore, the measurement of the missing transverse momentum  $\vec{p}_{T,miss}$  provides two additional constraints

$$\vec{P}_{0T}^{(1)} + \vec{P}_{0T}^{(2)} = \vec{p}_{T,miss} \quad (2.11)$$

on the unknown transverse momentum components  $\vec{P}_{0T}^{(k)}$ . Therefore, the total number of measurements is

$$N_m = 2(n+1) + 2 = 2n + 4 \quad (2.12)$$

and the number of undetermined parameters for any given event is readily obtained from (2.7) and (2.12)

$$N_p - N_m = 5 - n. \quad (2.13)$$

However, one might do better than this, by combining the information from two or more events [18, 19]. For example, consider another event of the same type. Since the  $n+1$  unknown masses were already counted in eq. (2.7), the second event introduces only 8 new parameters (the 4-momenta of the two  $X_0$  particles in the second event), bringing up the total number of unknowns in the two events to

$$N_p = 8 + 8 + (n+1) = n + 17. \quad (2.14)$$

At the same time, the constraints (2.10) and (2.11) are still valid for the second event, which results in  $2n+4$  additional constraints. This brings the total number of constraints to

$$N_m = (2n+4) + (2n+4) = 4n + 8. \quad (2.15)$$

Subtracting (2.14) and (2.15), we get

$$N_p - N_m = 9 - 3n. \quad (2.16)$$

Comparing our previous result (2.13) with (2.16), we see that the latter decreases much faster with  $n$ , therefore, when using the polynomial method, combining information from two different events is beneficial for large  $n$  (in this example, for  $n \geq 3$ ).

Following the same logic, one can generalize this parameter counting to the case where the polynomial method is applied for sets of  $N_{ev}$  different events at a time. The number of unknown parameters is

$$N_p = n + 1 + 8N_{ev}, \quad (2.17)$$

the number of constraints is

$$N_m = (2n+4)N_{ev}, \quad (2.18)$$

and therefore, the number of undetermined parameters is given by

$$N_p - N_m = n + 1 - 2(n-2)N_{ev}. \quad (2.19)$$

For  $N_{ev} = 1$  and  $N_{ev} = 2$  this equation reduces to (2.13) and (2.16), respectively. What is the optimal number of events  $N_{ev}$  for the polynomial method? The answer can be readily obtained from eq. (2.19), where  $N_{ev}$  enters the last term on the right-hand side. If this term is negative, increasing  $N_{ev}$  would decrease the number of undetermined parameters, therefore it would be beneficial to combine information from more and more different events. From eq. (2.19) we see that this would be case if the decay chain is sufficiently long, i.e.  $n \geq 3$ . On the other hand, when  $n = 1$ , considering more than one event at a time is actually detrimental - we are adding more unknowns than constraints. In the case of  $n = 2$ , the number of undetermined parameters  $N_p - N_m$  is actually independent of  $N_{ev}$  and one might as well consider the simplest case of  $N_{ev} = 1$ .

Let us now analyze how successful the polynomial method will be for different decay chain lengths. The number of undetermined parameters (2.16) for  $N_{ev} = 2$  is plotted in Fig. 2 with blue  $\times$  symbols, connected with blue line segments. We see that the polynomial method will be successful in determining all the masses of the BSM particles only if  $n \geq 3$ . For  $n = 1$  or  $n = 2$ , there will not be enough measurements for a complete mass determination<sup>3</sup> and the best one can do in that case is to obtain a *range of possible values* for the masses  $M_0$ ,  $M_1$  and  $M_2$  [27]. Recall that in the previous subsection we reached a similar conclusion regarding the endpoint method. Therefore, we see that both the endpoint and the polynomial methods, when used in isolation, would fail whenever the decay chain is rather short:  $n = 1$  or  $n = 2$ . This represents a definite problem, since there is no guarantee that the new physics would exhibit a long ( $n \geq 3$ ) decay chain. Therefore it is worth investigating whether there is an alternative method which would be successful in those two cases, i.e.  $n \leq 2$ .

One immediate idea which comes to mind is to use a hybrid method, i.e. combining the techniques of the polynomial and endpoint methods [34]. The parameter count in that case is very easy to do. The number of unknown parameters is the same as in the polynomial method:

$$N_p = n + 1 + 8N_{ev} . \quad (2.20)$$

Now, however, we need to account for the extra measurements (2.5) which are available from the endpoint method. Therefore, the total number of measurements for a hybrid method of this type is the sum of (2.5) and (2.18):

$$N_m = 2^n - (n + 1) + (2n + 4)N_{ev} . \quad (2.21)$$

Subtracting (2.20) and (2.21), we get

$$N_p - N_m = 2(n + 1) - 2^n - 2(n - 2)N_{ev} . \quad (2.22)$$

In Fig. 2, this quantity is plotted for fixed  $N_{ev} = 2$  with magenta  $\otimes$  symbols. We see that, even though the hybrid method performs better than the individual endpoint and polynomial methods, it still cannot solve the problem of masses for  $n = 2$ ! Therefore, a different approach

---

<sup>3</sup>As can be seen from the more general expression (2.19), this conclusion will not change even if we consider arbitrarily large number of events  $N_{ev}$ .

is needed. We shall now argue that the  $M_{T_2}$  method might just provide the solution to this problem in the  $n = 2$  case. What is more, we shall show that the  $M_{T_2}$  method can do that all *by itself*, without using any information derived from the endpoint or polynomial methods.

### 2.3 $M_{T_2}$ method

Here the number of unknown parameters is still

$$N_p = n + 1 . \quad (2.23)$$

In the next section we shall prove that, once we consider the notion of subsystem  $M_{T_2}^{(n,p,c)}$ , the total number of  $M_{T_2}$ -type endpoint measurements is

$$N_m = \frac{1}{6}n(n+1)(n+2) . \quad (2.24)$$

Then the number of undetermined parameters with this method is

$$N_p - N_m = \frac{1}{6}(n+1)(6 - 2n - n^2) , \quad (2.25)$$

which is plotted with green square symbols in Fig. 2. We see that for  $n \leq 3$ , the  $M_{T_2}$  method is by far the most powerful, and more importantly, it is the only method which is able to handle the problematic case of  $n = 2$ !

### 3. Defining a subsystem $M_{T_2}$ variable

The idea for a subsystem  $M_{T_2}$  was first discussed in [41] and applied in [45] for a specific supersymmetry example (associated squark-gluino production and decay). Here we shall generalize that concept for a completely general decay chain. For this purpose, let us redraw Fig. 1 as shown in Fig. 3. The subsystem  $M_{T_2}$  variable will be defined for the subchain inside the blue (yellow-shaded) box in Fig. 3. Before we give a formal definition of the subsystem  $M_{T_2}$  variables, let us first introduce some terminology for the BSM particles appearing in the decay chain. We shall find it convenient to distinguish the following types of BSM particles:

- “*Grandparents*”. Those are the two BSM particles  $X_n$  at the very top of the decay chains in Fig. 3. Since we have assumed symmetric events, the two grandparents in each event are identical, and carry the same index  $n$ . Of course, one may relax this assumption, and consider asymmetric events, as was done in [36, 45]. Then, the two “grandparents” will be different, and one would simply need to keep track of two separate grandparent indices  $n^{(1)}$  and  $n^{(2)}$ .
- “*Parents*”. Those are the two BSM particles  $X_p$  at the top of the subchain used to define the subsystem  $M_{T_2}$  variable. In Fig. 3 this subchain is identified by the blue (yellow-shaded) rectangular box. The idea behind the subsystem  $M_{T_2}$  is simply to apply the usual  $M_{T_2}$  definition for the subchain inside this box. Notice that the  $M_{T_2}$  concept usually requires the parents to be identical, therefore here we will characterize them by a single “parent” index  $p$ .

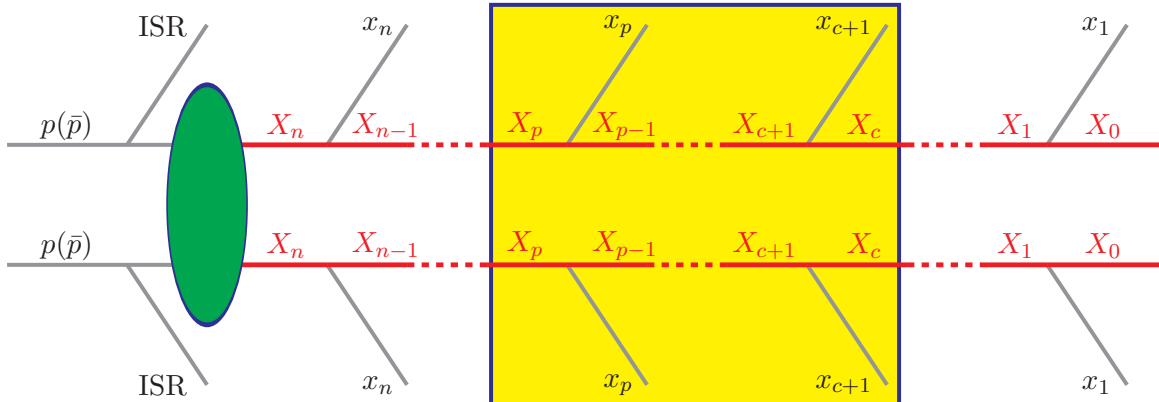


**Figure 3:** An alternative representation of Fig. 1, which illustrates the meaning of the subsystem  $M_{T2}^{(n,p,c)}$  variable defined in eq. (3.3).

- “*Children*”. Those are the two BSM particles  $X_c$  at the very end of the subchain used to define the subsystem  $M_{T2}$  variable, as indicated by the blue (yellow-shaded) rectangular box in Fig. 3. The children are also characterized by a single index  $c$ . In general, the true mass  $M_c$  of the two children is unknown. As usual, when calculating the value of the  $M_{T2}$  variable, one needs to choose a child “test” mass, which we shall denote with a tilde,  $\tilde{M}_c$ , in order to distinguish it from the true mass  $M_c$  of  $X_c$ .
- *Dark matter candidates*. Those are the two stable neutral particles  $X_0$  appearing at the very end of the cascade chain. We see that while those are the particles responsible for the measured missing momentum in the event (see eq. (2.11)), they are relevant for  $M_{T2}$  only in the special case of  $c = 0$ .

With those definitions, we are now ready to generalize the conventional  $M_{T2}$  definition [13, 17]. From Fig. 3 we see that any subchain is specified by the parent index  $p$  and the child index  $c$ , while the total length of the whole chain (and thus the type of event) is given by the grandparent index  $n$ . Therefore, the subsystem  $M_{T2}$  variable will have to carry those three indices as well, and we shall use the notation  $M_{T2}^{(n,p,c)}$ . In the following we shall refer to this generalized quantity as either “subsystem” or “subchain”  $M_{T2}$ . It is clear that the set of three indices  $(n, p, c)$  must be ordered as follows:

$$n \geq p > c \geq 0 . \quad (3.1)$$

We shall now give a formal definition of the quantity  $M_{T2}^{(n,p,c)}$ , generalizing the original idea of  $M_{T2}$  [13, 17]. The parent and child indices  $p$  and  $c$  uniquely define a subchain, within which one can form the transverse masses  $M_T^{(1)}$  and  $M_T^{(2)}$  of the two parents:

$$M_T^{(k)}(p_p^{(k)}, p_{p-1}^{(k)}, \dots, p_{c+1}^{(k)}, \vec{P}_{cT}^{(k)}; \tilde{M}_c), \quad k = 1, 2 . \quad (3.2)$$

Here  $p_i^{(k)}$ ,  $c+1 \leq i \leq p$ , are the measured 4-momenta of the SM particles within the subchain,  $\vec{P}_{cT}^{(k)}$  are the unknown transverse momenta of the children, while  $\tilde{M}_c$  is their unknown (test)

mass. Then, the subsystem  $M_{T_2}^{(n,p,c)}$  is defined by minimizing the larger of the two transverse masses (3.2) over the allowed values of the children's transverse momenta  $\vec{P}_{cT}^{(k)}$ :

$$M_{T_2}^{(n,p,c)}(\tilde{M}_c) = \min_{\sum_{k=1}^2 \vec{P}_{cT}^{(k)} = -\sum_{k=1}^2 \sum_{j=c+1}^n \vec{p}_{jT}^{(k)} - \vec{p}_T} \left\{ \max \left\{ M_T^{(1)}, M_T^{(2)} \right\} \right\}, \quad (3.3)$$

where  $\vec{p}_T$  indicates any additional transverse momentum due to initial state radiation (ISR) (see Figs. 1 and 3). Notice that in this definition, the dependence on the grandparent index  $n$  enters only through the restriction on the children's transverse momenta  $\vec{P}_{cT}^{(k)}$ . Using momentum conservation in the transverse plane

$$\sum_{k=1}^2 \vec{P}_{0T}^{(k)} + \sum_{k=1}^2 \sum_{j=1}^n \vec{p}_{jT}^{(k)} + \vec{p}_T = 0, \quad (3.4)$$

we can rewrite the restriction on the children's transverse momenta  $\vec{P}_{cT}^{(k)}$  as

$$\sum_{k=1}^2 \vec{P}_{cT}^{(k)} = \sum_{k=1}^2 \vec{P}_{0T}^{(k)} + \sum_{k=1}^2 \sum_{j=1}^c \vec{p}_{jT}^{(k)} = \vec{p}_{T,miss} + \sum_{k=1}^2 \sum_{j=1}^c \vec{p}_{jT}^{(k)}, \quad (3.5)$$

where in the last step we used eq. (2.11). Eq. (3.5) allows us to rewrite the subsystem  $M_{T_2}^{(n,p,c)}$  definition (3.3) in a form which does not manifestly depend on the grandparent index  $n$ :

$$M_{T_2}^{(n,p,c)}(\tilde{M}_c) = \min_{\sum_{k=1}^2 \vec{P}_{cT}^{(k)} = \vec{p}_{T,miss} + \sum_{k=1}^2 \sum_{j=1}^c \vec{p}_{jT}^{(k)}} \left\{ \max \left\{ M_T^{(1)}, M_T^{(2)} \right\} \right\}. \quad (3.6)$$

However, the grandparent index  $n$  is still implicitly present through the global quantity  $\vec{p}_{T,miss}$ , which knows about the whole event. We shall see below that the interpretation of the experimentally observable endpoints, kinks, etc., for the so defined subsystem  $M_{T_2}^{(n,p,c)}$  quantity, does depend on the grandparent index  $n$ , which justifies our notation.

We are now in a position to compare our subsystem  $M_{T_2}^{(n,p,c)}$  quantity to the conventional  $M_{T_2}$  variable. The latter is nothing but the special case of  $n = p$  and  $c = 0$ :

$$M_{T_2} \equiv M_{T_2}^{(n,n,0)}, \quad (3.7)$$

i.e. the conventional  $M_{T_2}$  is simply characterized by a single integer  $n$ , which indicates the length of the decay chain. We see that we are generalizing the conventional  $M_{T_2}$  variable in two different aspects: first, we are allowing the parents  $X_p$  to be different from the particles  $X_n$  originally produced in the event (the grandparents), and second, we are allowing the children  $X_c$  to be different from the dark matter particles  $X_0$  appearing at the end of the cascade chain and responsible for the missing energy. The benefits of this generalization will become apparent in the next section, where we shall discuss the available measurements from the different subsystem  $M_{T_2}^{(n,p,c)}$  variables.

In conclusion of this section, let us derive the result (2.24) used in Section 2.3. We count how many different subsystem  $M_{T_2}^{(n,p,c)}$  quantities (3.3) exist for a given maximum value  $n$

of the grandparent index. First, pick a parent index  $p$ , which can range from 1 to  $n$ . Then, for this fixed value of  $p$ , the child index  $c$  can take a total of  $p$  values:  $0 \leq c \leq p - 1$ , while the grandparent index can take<sup>4</sup> a total of  $n - p + 1$  values. Therefore, the total number of allowed combinations  $(n, p, c)$  is

$$\sum_{p=1}^n p(n-p+1) = \frac{1}{6} n(n+1)(n+2), \quad (3.8)$$

in agreement with (2.24).

#### 4. A short decay chain $X_2 \rightarrow X_1 \rightarrow X_0$

As we already discussed in Sec. 2, a relatively long ( $n \geq 3$ ) new physics decay chain can be handled by a variety of mass measurement methods, and in principle a complete determination of the mass spectrum in that case *is possible* at a hadron collider. We also showed that a relatively short ( $n = 1$  or  $n = 2$ ) decay chain would present a major challenge, and a complete mass determination might be possible only through  $M_{T2}$  methods. From now on we shall therefore concentrate only on this most problematic case of  $n \leq 2$ .

First let us summarize what types of subsystem  $M_{T2}^{(n,p,c)}$  measurements are available in the case of  $n \leq 2$ . According to eq. (3.8), there exist a total of 4 different  $M_{T2}^{(n,p,c)}$  quantities, which are illustrated in Fig. 4. Each  $M_{T2}^{(n,p,c)}$  distribution would exhibit an upper endpoint  $M_{T2,max}^{(n,p,c)}$ , whose measurement would provide one constraint on the physical masses. In order to be able to invert and solve for the masses of the new particles in terms of the measured endpoints, we need to know the analytical expressions relating the endpoints  $M_{T2,max}^{(n,p,c)}$  to the physical masses  $M_i$ . In this section we summarize those relations for each  $M_{T2}^{(n,p,c)}$  quantity with  $n \leq 2$ . Some of these results (e.g. portions of Secs. 4.1 and Secs. 4.3) have already appeared in the literature, and we include them here for completeness. The discussion in Secs. 4.2 and Secs. 4.4, on the other hand, is new. In all cases, we shall allow for the presence of an arbitrary transverse momentum  $p_T$  due to ISR. This represents a generalization of all existing results in the literature, which have been derived in the two special cases  $p_T = 0$  [32] or  $p_T = \infty$  [31].

We shall find it convenient to write the formulas for the endpoints  $M_{T2,max}^{(n,p,c)}$  not in terms of the actual masses, but in terms of the mass parameters

$$\mu_{(n,p,c)} \equiv \frac{M_n}{2} \left( 1 - \frac{M_c^2}{M_p^2} \right). \quad (4.1)$$

---

<sup>4</sup>Note that different values of the grandparent index  $n$  correspond to different types of events. For example, in order to study the  $M_{T2}^{(n_1,p,c)}$  variables for some given  $n_1$ , we must look at events of  $X_{n_1}$  pair-production, while in order to form the  $M_{T2}^{(n_2,p,c)}$  distributions for another value  $n_2 < n_1$ , we must look at events of  $X_{n_2}$  pair-production. Because of the mass hierarchy (2.1), the observation of events of the former type ( $X_{n_1}$  pair-production) guarantees that the collider will eventually be able to also produce events of the latter type ( $X_{n_2}$  pair-production). Therefore, the relevant integer for our count is the maximum value of  $n$  achievable at a given collider experiment.

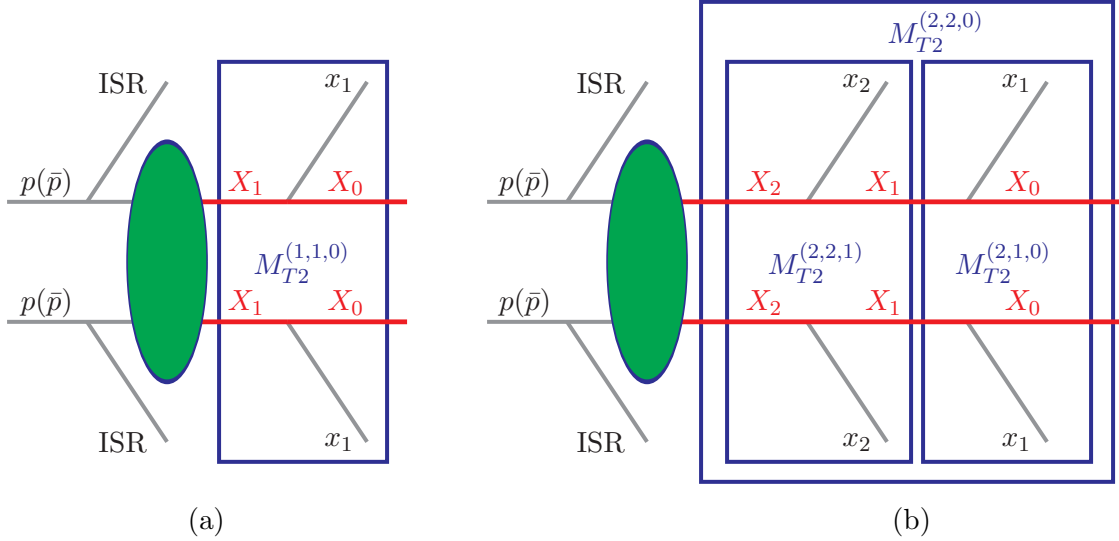


**Figure 4:** The subsystem  $M_{T_2}^{(n,p,c)}$  variables which are available for (a)  $n = 1$  and (b)  $n = 2$  events.

The advantage of using this shorthand notation will become apparent very shortly. Notice that not all of the  $\mu$  parameters defined in (4.1) are independent. For a given maximum value of  $n$ , the total number of  $\mu$  parameters from (4.1) is the same as the total number of subsystem  $M_{T_2}$  variables and is given by (2.24). All of those  $\mu$  parameters are functions of just  $n + 1$  masses  $M_i$ ,  $0 \leq i \leq n$ , as indicated by eq. (2.23). Therefore, the  $\mu$  parameters must obey certain relations, whose number is given by (2.25). For example, for  $n \leq 2$ , we have a total of four  $\mu$  parameters:  $\mu_{(1,1,0)}$ ,  $\mu_{(2,1,0)}$ ,  $\mu_{(2,2,0)}$  and  $\mu_{(2,2,1)}$ , and only three masses:  $M_0$ ,  $M_1$  and  $M_2$ , so that there is one constraint:

$$\mu_{(2,1,0)} (\mu_{(2,2,0)} - \mu_{(2,2,1)}) = \mu_{(1,1,0)}^2 . \quad (4.2)$$

#### 4.1 The subsystem variable $M_{T_2}^{(1,1,0)}$

We start with the simplest case of  $n = 1$  shown in Fig. 4(a). Here  $M_{T_2}^{(1,1,0)}$  is the only possibility, and it coincides with the conventional  $M_{T_2}$  variable, as indicated by (3.7). Therefore, the previous results in the literature which have been derived for the conventional  $M_{T_2}$  variable (3.7), would still apply. In particular, in the limit of  $p_T = 0$ , the upper endpoint  $M_{T_2,max}^{(1,1,0)}$  depends on the test mass  $\tilde{M}_0$  as follows [32]

$$M_{T_2,max}^{(1,1,0)}(\tilde{M}_0, p_T = 0) = \mu_{(1,1,0)} + \sqrt{\mu_{(1,1,0)}^2 + \tilde{M}_0^2} , \quad (4.3)$$

where the parameter  $\mu_{(1,1,0)}$  is defined in terms of the physical masses  $M_1$  and  $M_0$  according to eq. (4.1):

$$\mu_{(1,1,0)} \equiv \frac{M_1}{2} \left( 1 - \frac{M_0^2}{M_1^2} \right) = \frac{M_1^2 - M_0^2}{2M_1} . \quad (4.4)$$

As usual, the endpoint (4.3) can be interpreted as the mass  $M_1$  of the parent particle  $X_1$ , so that eq. (4.3) provides a relation between the masses of  $X_0$  and  $X_1$ . In the early literature on  $M_{T_2}$ , this relation had to be derived numerically, by building the  $M_{T_2}$  distributions for



different values of the test mass  $\tilde{M}_0$ , and reading off their endpoints. Nowadays, with the work of Ref. [32], the relation is known analytically, and, as seen from (4.3), is parameterized by a single parameter  $\mu_{(1,1,0)}$ . Therefore, in order to extract the value of this parameter, we only need to perform a single measurement, i.e. we only need to study the  $M_{T2}$  distribution for *one* particular choice of the test mass  $\tilde{M}_0$ . We shall find it convenient to choose  $\tilde{M}_0 = 0$ , in which case eqs. (4.3) and (4.4) give

$$M_{T2,max}^{(1,1,0)}(\tilde{M}_0 = 0, p_T = 0) = 2\mu_{(1,1,0)} = \frac{M_1^2 - M_0^2}{M_1}, \quad (4.5)$$

providing the required measurement of the parameter  $\mu_{(1,1,0)}$ . Eq. (4.5) demonstrates the usefulness of the  $M_{T2}$  concept – just a single measurement of the endpoint of the  $M_{T2}$  distribution for a single fixed value of the test mass  $\tilde{M}_0$  is sufficient to provide us with one constraint among the unknown masses ( $M_1$  and  $M_0$  in this case).

Unfortunately, one single measurement (4.5) is not enough to pin down two different masses. In order to measure *both*  $M_0$  and  $M_1$ , without any theoretical assumptions or prejudice, we obviously need additional experimental input. From the general expression (4.3) it is clear that measuring other  $M_{T2,max}^{(1,1,0)}$  endpoints, for different values of the test mass  $\tilde{M}_0$ , will not help, since we will simply be measuring the same combination of masses  $\mu_{(1,1,0)}$  over and over again, obtaining no new information. Another possibility might be to consider events with the next longest decay chain ( $n = 2$ ), which, as advertised in the Introduction and shown below in Section 5, will be able to provide enough information for a complete mass determination of all particles  $X_0$ ,  $X_1$  and  $X_2$ . However, the existence and the observation of the  $n = 2$  decay chain is certainly not guaranteed – to begin with, the particles  $X_2$  may not exist, or they may have too low cross-sections. It is therefore of particular importance to ask the question whether the  $n = 1$  process in Fig. 4(a) alone can allow a determination of both  $M_0$  and  $M_1$ . As shown in Ref. [31], the answer to this question, at least in principle, is “Yes”, and what is more, one can achieve this using the very same  $M_{T2}$  variable  $M_{T2}^{(1,1,0)}$ .

The key is to realize that in reality at any collider, and especially at hadron colliders like the Tevatron and the LHC, there will be sizable contributions from initial state radiation (ISR) with nonzero  $p_T$ , where one or more jets are radiated off the initial state, before the hard scattering interaction. (In Figs. 1, 3 and 4 the green ellipse represents the hard scattering, while “ISR” stands for a generic ISR jet.). This effect leads to a drastic change in the behavior of the  $M_{T2,max}^{(1,1,0)}(\tilde{M}_0, p_T)$  function, which starts to exhibit a kink at the true location of the child mass  $\tilde{M}_0 = M_0$ :

$$\left( \frac{\partial M_{T2,max}^{(1,1,0)}(\tilde{M}_0, p_T)}{\partial \tilde{M}_0} \right)_{\tilde{M}_0 = M_0 - \epsilon} \neq \left( \frac{\partial M_{T2,max}^{(1,1,0)}(\tilde{M}_0, p_T)}{\partial \tilde{M}_0} \right)_{\tilde{M}_0 = M_0 + \epsilon}, \quad (4.6)$$

and furthermore, the value of  $M_{T2,max}^{(1,1,0)}$  at that point reveals the true mass of the parent as well:

$$M_{T2,max}^{(1,1,0)}(\tilde{M}_0 = M_0, p_T) = M_1. \quad (4.7)$$

This kink feature (4.6,4.7) was observed and illustrated in Ref. [31] (see their Sec. 4.4). We find that it can also be understood analytically, by generalizing the result (4.3) to account for the additional ISR transverse momentum  $\vec{p}_T$ . Recall that eq. (4.3) was derived in Ref. [32] under the assumption that the missing transverse momentum due to the two escaping particles  $X_0$  is exactly balanced by the transverse momenta of the two visible particles  $x_1$  used to form  $M_{T2}^{(1,1,0)}$ :

$$\vec{P}_{0T}^{(1)} + \vec{P}_{0T}^{(2)} + \vec{p}_{1T}^{(1)} + \vec{p}_{1T}^{(2)} = 0 . \quad (4.8)$$

We may sometimes refer to this situation as a ‘‘balanced’’ momentum configuration<sup>5</sup>. In the presence of ISR with some non-zero transverse momentum  $\vec{p}_T$ , eq. (4.8) in general ceases to be valid, and is modified to

$$\vec{P}_{0T}^{(1)} + \vec{P}_{0T}^{(2)} + \vec{p}_{1T}^{(1)} + \vec{p}_{1T}^{(2)} = -\vec{p}_T , \quad (4.9)$$

in accordance with (3.4). Including the ISR effects, we find that the expression (4.3) for the  $M_{T2,max}^{(1,1,0)}$  endpoint splits into two branches

$$M_{T2,max}^{(1,1,0)}(\tilde{M}_0, p_T) = \begin{cases} F_L^{(1,1,0)}(\tilde{M}_0, p_T) , & \text{if } \tilde{M}_0 \leq M_0 , \\ F_R^{(1,1,0)}(\tilde{M}_0, p_T) , & \text{if } \tilde{M}_0 \geq M_0 , \end{cases} \quad (4.10)$$

where

$$F_L^{(1,1,0)}(\tilde{M}_0, p_T) = \left\{ \left[ \mu_{(1,1,0)}(p_T) + \sqrt{\left( \mu_{(1,1,0)}(p_T) + \frac{p_T}{2} \right)^2 + \tilde{M}_0^2} \right]^2 - \frac{p_T^2}{4} \right\}^{\frac{1}{2}} , \quad (4.11)$$

$$F_R^{(1,1,0)}(\tilde{M}_0, p_T) = \left\{ \left[ \mu_{(1,1,0)}(-p_T) + \sqrt{\left( \mu_{(1,1,0)}(-p_T) - \frac{p_T}{2} \right)^2 + \tilde{M}_0^2} \right]^2 - \frac{p_T^2}{4} \right\}^{\frac{1}{2}} , \quad (4.12)$$

and the  $p_T$ -dependent parameter  $\mu_{(1,1,0)}(p_T)$  is defined as

$$\mu_{(1,1,0)}(p_T) = \mu_{(1,1,0)} \left( \sqrt{1 + \left( \frac{p_T}{2M_1} \right)^2} - \frac{p_T}{2M_1} \right) . \quad (4.13)$$

Both branches correspond to extreme momentum configurations in which all three transverse vectors  $\vec{p}_{1T}^{(1)}$ ,  $\vec{p}_{1T}^{(2)}$  and  $\vec{p}_T$  are collinear. The difference is that the left branch  $F_L^{(1,1,0)}$  corresponds to the configuration  $(\vec{p}_{1T}^{(1)} \uparrow \vec{p}_{1T}^{(2)}) \uparrow \vec{p}_T$ , while the right branch  $F_R^{(1,1,0)}$  corresponds to  $(\vec{p}_{1T}^{(1)} \uparrow \vec{p}_{1T}^{(2)}) \uparrow \vec{p}_T$ . Therefore, the two branches are simply related as

$$F_R^{(1,1,0)}(\tilde{M}_0, p_T) = F_L^{(1,1,0)}(\tilde{M}_0, -p_T) . \quad (4.14)$$

It is easy to verify that in the absence of ISR, (i.e. for  $p_T = 0$ ) our general result (4.10) reduces to the previous formula (4.3).

---

<sup>5</sup>This should not be confused with the term ‘‘balanced’’ used for the analytic  $M_{T2}$  solutions discussed in [28, 32].

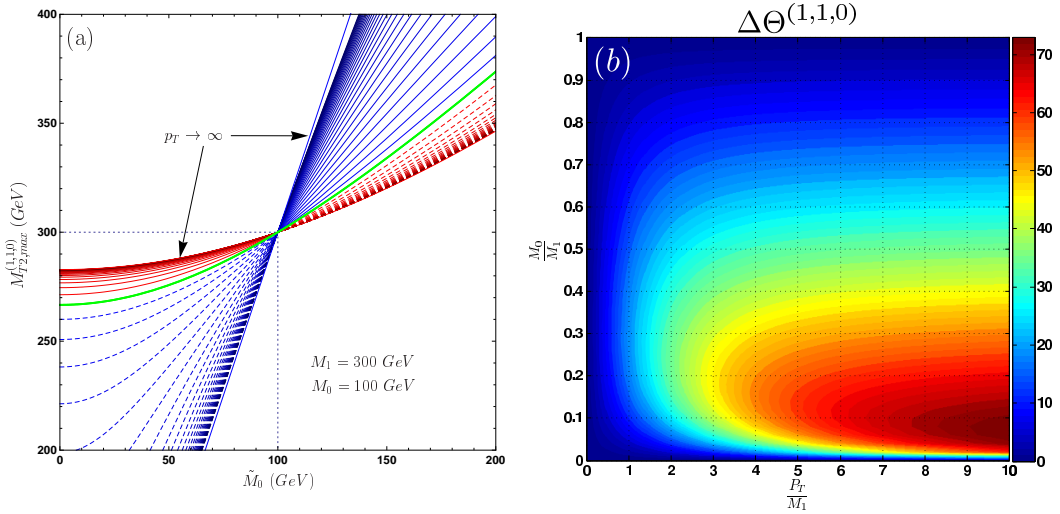


**Figure 5:** (a) Dependence of the  $M_{T2,max}^{(1,1,0)}$  upper kinematic endpoint (solid lines) on the value of the test mass  $\tilde{M}_0$ , for  $M_1 = 300$  GeV, and  $M_0 = 100$  GeV, and for different values of the transverse momentum  $p_T$  of the ISR jet, starting from  $p_T = 0$  (green line), and increasing up to  $p_T = 3$  TeV in increments of  $\Delta p_T = 100$  GeV, from bottom to top. The uppermost line corresponds to the limiting case  $p_T \rightarrow \infty$ . The horizontal (vertical) dotted line denotes the true value of the parent (child) mass. Solid (dashed) lines indicate true (false) endpoints. The red lines correspond to the function  $F_L^{(1,1,0)}$  defined in eq. (4.11), while the blue lines correspond to the function  $F_R^{(1,1,0)}$  defined in eq. (4.12). (b) The value of the kink  $\Delta\Theta^{(1,1,0)}$  defined in (4.21), as a function of the dimensionless ratios  $\frac{p_T}{M_1}$  and  $\frac{M_0}{M_1}$ .

Our result (4.10) for the  $M_{T2,max}^{(1,1,0)}$  upper kinematic endpoint as a function of the test mass  $\tilde{M}_0$  is illustrated in Fig. 5(a). We have chosen the same mass spectrum ( $M_0 = 100$  GeV and  $M_1 = 300$  GeV) as the one used in Ref. [31], so that our Fig. 5(a) can be directly compared to Fig. 9 of Ref. [31]. We consider a single ISR jet and show results for several different values of its transverse momentum  $p_T$ , starting from  $p_T = 0$  (the green solid line) and increasing the value of  $p_T$  in increments of  $\Delta p_T = 100$  GeV. The uppermost solid line corresponds to the limiting case  $p_T \rightarrow \infty$ . The true value of the parent (child) mass is marked by the horizontal (vertical) dotted line. The red (blue) lines correspond to the function  $F_L^{(1,1,0)}$  ( $F_R^{(1,1,0)}$ ). The solid portions of those lines correspond to the true  $M_{T2,max}^{(1,1,0)}$  endpoint, while the dashed segments are simply the extension of  $F_L^{(1,1,0)}$  and  $F_R^{(1,1,0)}$  into the “wrong” region for  $\tilde{M}_0$ , giving a false endpoint.

Fig. 5(a) reveals that the two branches (4.11) and (4.12) always cross at the point  $(M_0, M_1)$ , in agreement with eq. (4.7). Interestingly, the sharpness of the resulting kink at  $\tilde{M}_0 = M_0$  depends on the hardness of the ISR jet, as can be seen directly from (4.10). For small  $p_T$ , the kink is barely visible, and in the limit  $p_T \rightarrow 0$  we obtain the old result (4.3) for the “balanced” momentum configuration, shown with the green solid line, which does not exhibit any kink. In the other extreme, at very large  $p_T$ , we see a pronounced kink, which has a well-defined limit as  $p_T \rightarrow \infty$ . Our results in this regard are in agreement with the

findings of Ref. [31].

The  $M_{T2,max}^{(1,1,0)}$  kink exhibited in eq. (4.10) and in Fig. 5(a) is our first, but not last, encounter with a kink feature in an  $M_{T2}^{(n,p,c)}$  variable. Below we shall see that the  $M_{T2}$  kinks are rather common phenomena, and we shall encounter at least two other kink types by the end of Sec. 4. Therefore, we find it convenient to quantify the sharpness of any such kink as follows. Consider a generic subsystem  $M_{T2}^{(n,p,c)}$  variable whose endpoint  $M_{T2,max}^{(n,p,c)}(\tilde{M}_c, p_T)$  exhibits a kink:

$$M_{T2,max}^{(n,p,c)}(\tilde{M}_c, p_T) = \begin{cases} F_L^{(n,p,c)}(\tilde{M}_c, p_T), & \text{if } \tilde{M}_c \leq M_c, \\ F_R^{(n,p,c)}(\tilde{M}_c, p_T), & \text{if } \tilde{M}_c \geq M_c. \end{cases} \quad (4.15)$$

The kink appears because  $M_{T2,max}^{(n,p,c)}(\tilde{M}_c, p_T)$  is not given by a single function, but has two separate branches. The first (“low”) branch applies for  $\tilde{M}_c \leq M_c$ , and is given by some function  $F_L^{(n,p,c)}(\tilde{M}_c, p_T)$ , while the second (“high”) branch is valid for  $\tilde{M}_c \geq M_c$ , and is given by a different function,  $F_R^{(n,p,c)}(\tilde{M}_c, p_T)$ . The function  $M_{T2,max}^{(n,p,c)}(\tilde{M}_c, p_T)$  itself is continuous and the two branches coincide at  $\tilde{M}_c = M_c$ :

$$F_L^{(n,p,c)}(M_c, p_T) = F_R^{(n,p,c)}(M_c, p_T), \quad (4.16)$$

but their *derivatives* do not match:

$$\left( \frac{\partial F_L^{(n,p,c)}}{\partial \tilde{M}_c} \right)_{\tilde{M}_c=M_c} \neq \left( \frac{\partial F_R^{(n,p,c)}}{\partial \tilde{M}_c} \right)_{\tilde{M}_c=M_c}, \quad (4.17)$$

leading to the appearance of the kink. Let us define the left and right slope of the  $M_{T2,max}^{(n,p,c)}(\tilde{M}_c, p_T)$  function at  $\tilde{M}_c = M_c$  in terms of two angles  $\Theta_L^{(n,p,c)}$  and  $\Theta_R^{(n,p,c)}$ , correspondingly:

$$\tan \Theta_L^{(n,p,c)} \equiv \left( \frac{\partial F_L^{(n,p,c)}(\tilde{M}_c)}{\partial \tilde{M}_c} \right)_{\tilde{M}_c=M_c}, \quad (4.18)$$

$$\tan \Theta_R^{(n,p,c)} \equiv \left( \frac{\partial F_R^{(n,p,c)}(\tilde{M}_c)}{\partial \tilde{M}_c} \right)_{\tilde{M}_c=M_c}. \quad (4.19)$$

Now we shall define the amount of kink as the angular difference  $\Delta\Theta^{(n,p,c)}$  between the two branches:

$$\Delta\Theta^{(n,p,c)} \equiv \Theta_R^{(n,p,c)} - \Theta_L^{(n,p,c)} = \arctan \left( \frac{\tan \Theta_R^{(n,p,c)} - \tan \Theta_L^{(n,p,c)}}{1 + \tan \Theta_R^{(n,p,c)} \tan \Theta_L^{(n,p,c)}} \right). \quad (4.20)$$

A large value of  $\Delta\Theta^{(n,p,c)}$  implies that the relative angle between the low and high branches at the point of their junction  $\tilde{M}_c = M_c$  is also large, and in that sense the kink would be more pronounced and relatively easier to see.

This definition can be immediately applied to the  $M_{T2,max}^{(1,1,0)}$  kink that we just discussed. Substituting the formulas (4.11) and (4.12) for the two branches  $F_L^{(1,1,0)}$  and  $F_R^{(1,1,0)}$  into

the definitions (4.18,4.19) and subsequently into (4.20), we obtain an expression for the size  $\Delta\Theta^{(1,1,0)}$  of the  $M_{T2,max}^{(1,1,0)}$  kink:

$$\Delta\Theta^{(1,1,0)} = \arctan \left( \frac{M_0 (M_1^2 - M_0^2) p_T \sqrt{4M_1^2 + p_T^2}}{M_1 (M_1^2 - M_0^2)^2 + 2M_0^2 M_1 (4M_1^2 + p_T^2)} \right). \quad (4.21)$$

The result (4.21) is illustrated numerically in Fig. 5(b). As can be seen from (4.21),  $\Delta\Theta^{(1,1,0)}$  depends on the two masses  $M_0$  and  $M_1$ , as well as the size of the ISR  $p_T$ . However, since  $\Delta\Theta^{(1,1,0)}$  is a dimensionless quantity, its dependence on those three parameters can be simply illustrated in terms of the dimensionless ratios  $\frac{p_T}{M_1}$  and  $\frac{M_0}{M_1}$ . This is why in Fig. 5(b) we plot  $\Delta\Theta^{(1,1,0)}$  (in degrees) as a function of  $\frac{p_T}{M_1}$  and  $\frac{M_0}{M_1}$ .

Fig. 5(b) confirms that the kink develops at large  $p_T$ , and is completely absent at  $p_T = 0$ , a result which may have already been anticipated on the basis of Fig. 5(a). For any given mass ratio  $\frac{M_0}{M_1}$ , the kink is largest for the hardest possible  $p_T$ . In the limit  $p_T \rightarrow \infty$  we obtain

$$\lim_{p_T \rightarrow \infty} \Delta\Theta^{(1,1,0)} = \arctan \left( \frac{M_1^2 - M_0^2}{2M_0 M_1} \right), \quad (4.22)$$

in agreement with the result obtained in [31]. From Fig. 5(b) one can see that at sufficiently large  $p_T$ , the  $\Delta\Theta^{(1,1,0)}$  contours become almost horizontal, i.e. the size of the kink  $\Delta\Theta^{(1,1,0)}$  becomes very weakly dependent on  $p_T$ . A careful examination of the figure reveals that the asymptotic behavior at  $p_T \rightarrow \infty$  is in agreement with the analytical result (4.22). Notice that the maximum possible value of any kink of the type (4.15) is  $\Delta\Theta_{max}^{(n,p,c)} = 90^\circ$ . According to Fig. 5(b) and eq. (4.22), in the case of  $\Delta\Theta^{(1,1,0)}$  the absolute maximum can be obtained only in the  $p_T \rightarrow \infty$  and  $M_0 \rightarrow 0$  limit. The former condition will never be realized in a realistic experiment, while the latter condition makes the observation of the kink rather problematic, since the “low” branch  $F_L$  of the  $M_{T2,max}^{(1,1,0)}(\tilde{M}_0, p_T)$  function is too short to be observed experimentally. Therefore, under realistic circumstances, we would expect the size of the kink  $\Delta\Theta^{(1,1,0)}$  to be only on the order of a few tens of degrees, which are the more typical values seen in Fig. 5(b).

According to Fig. 5(b), for a given fixed  $p_T$ , the sharpness of the  $\Delta\Theta^{(1,1,0)}$  kink depends on the mass hierarchy of the particles  $X_1$  and  $X_0$ . When they are relatively degenerate, i.e. their mass ratio  $\frac{M_0}{M_1}$  is large, the kink is relatively small. Conversely, when  $X_0$  is much lighter than  $X_1$ , the kink is more pronounced. The optimum mass ratio  $\frac{M_0}{M_1}$  which maximizes the kink for a given  $p_T$ , is rather weakly dependent on the  $p_T$ , and for  $p_T \rightarrow \infty$  eventually goes to zero, in agreement with eq. (4.22). However, for more reasonable values of  $p_T$  as the ones shown on the left half of the plot, the optimal ratio  $\frac{M_0}{M_1}$  varies between 0.3 (at  $p_T \sim 0$ ) to 0.1 (at  $p_T \sim 5M_1$ ). In this sense, the value of  $\frac{M_0}{M_1} = \frac{1}{3}$  which was chosen for the illustration in Fig. 5(a) (as well as Fig. 9 in Ref. [31]) is rather typical.

In conclusion of this subsection, it is worth summarizing the main points from it. The good news is that the  $\Delta\Theta^{(1,1,0)}$  kink in principle offers a second, independent piece of information about the masses of the particles  $X_0$  and  $X_1$ . When taken together with the  $M_{T2,max}^{(1,1,0)}$  endpoint measurement (4.5), it will allow us to determine *both* masses  $M_0$  and  $M_1$ ,

in a completely model-independent way. Our analytical results regarding the  $\Delta\Theta^{(1,1,0)}$  kink complement the study of Ref. [31], where this kink was first discovered. However, on the down side, we should mention that much of our discussion regarding the  $\Delta\Theta^{(1,1,0)}$  kink may be of limited practical interest, for several reasons. First, as seen in Fig. 5, the kink becomes visible only for sufficiently large values of the  $p_T$ . Since the ISR  $p_T$  spectrum is falling rather steeply, one would need to collect relatively large amounts of data, in order to guarantee the presence of events with sufficiently hard ISR jets. Even then, the collected events may not contain the momentum configuration required to give the maximum value of  $M_{T2}^{(1,1,0)}$ . An alternative approach to make use of the kink structure would be to measure the endpoint function  $M_{T2,max}^{(1,1,0)}(\tilde{M}_0, p_T)$  for several different  $p_T$  ranges, and then fit it to the analytical formula (4.10). Whether and how well this can work in practice, remains to be seen, but the results of [31] from a toy exercise in the absence of any backgrounds and detector resolution effects do not appear very encouraging. Nevertheless, while the kink structure  $\Delta\Theta^{(1,1,0)}$  may be difficult to observe, the measurement (4.5) of the endpoint  $M_{T2,max}^{(1,1,0)}(\tilde{M}_0 = 0, p_T = 0)$  should be relatively straightforward. In Secs. 5.1 and 5.3 we shall see that the additional  $M_{T2}$  information from events with  $n = 2$  decay chains will eventually allow us to determine all the unknown masses.

#### 4.2 The subsystem variable $M_{T2}^{(2,2,1)}$

The subsystem variable  $M_{T2}^{(2,2,1)}$  is illustrated in Fig. 4(b), where we use the subchain within the smaller rectangle on the left.  $M_{T2}^{(2,2,1)}$  is a genuine subchain variable in the sense that we only use the SM decay products  $x_2$ , and ignore any remaining objects arising from the two  $x_1$ 's. In the absence of ISR ( $p_T = 0$ ) one can adapt the results from [32] and show that the formula for the  $M_{T2}^{(2,2,1)}$  endpoint is

$$M_{T2,max}^{(2,2,1)}(\tilde{M}_1, p_T = 0) = \mu_{(2,2,1)} + \sqrt{\mu_{(2,2,1)}^2 + \tilde{M}_1^2}, \quad (4.23)$$

where the parameter  $\mu_{(2,2,1)}$  was defined in eq. (4.1):

$$\mu_{(2,2,1)} \equiv \frac{M_2}{2} \left( 1 - \frac{M_1^2}{M_2^2} \right) = \frac{M_2^2 - M_1^2}{2M_2}. \quad (4.24)$$

Almost all of our discussion from the previous Section 4.1 can be directly applied here as well. For example, in order to measure the parameter  $\mu_{(2,2,1)}$ , we only need to extract the endpoint of a *single* distribution, for a single fixed value of the test mass  $\tilde{M}_1$ . As before, we choose to use  $\tilde{M}_1 = 0$ . The resulting endpoint measurement

$$M_{T2,max}^{(2,2,1)}(\tilde{M}_1 = 0, p_T = 0) = 2\mu_{(2,2,1)} = \frac{M_2^2 - M_1^2}{M_2} \quad (4.25)$$

provides the required measurement of the parameter  $\mu_{(2,2,1)}$  appearing in eq. (4.23), as well as one constraint on the masses  $M_1$  and  $M_2$  involved in the problem. More importantly, the new constraint (4.25) is independent of the relation (4.5) found previously in Sec. 4.1.

The new variable  $M_{T2}^{(2,2,1)}$  will also exhibit a kink in the plot of its endpoint  $M_{T2,max}^{(2,2,1)}$  as a function of the test mass  $\tilde{M}_1$ . This is the same type of kink as the one discussed in

the previous subsection, therefore all of our previous results would apply here as well. In particular, the analytical expression for the kink is given by

$$M_{T2,max}^{(2,2,1)}(\tilde{M}_1, p_T) = \begin{cases} F_L^{(2,2,1)}(\tilde{M}_1, p_T), & \text{if } \tilde{M}_1 \leq M_1, \\ F_R^{(2,2,1)}(\tilde{M}_1, p_T), & \text{if } \tilde{M}_1 \geq M_1, \end{cases} \quad (4.26)$$

where

$$F_L^{(2,2,1)}(\tilde{M}_1, p_T) = \left\{ \left[ \mu_{(2,2,1)}(p_T) + \sqrt{\left( \mu_{(2,2,1)}(p_T) + \frac{p_T}{2} \right)^2 + \tilde{M}_1^2} \right]^2 - \frac{p_T^2}{4} \right\}^{\frac{1}{2}}, \quad (4.27)$$

$$F_R^{(2,2,1)}(\tilde{M}_1, p_T) = \left\{ \left[ \mu_{(2,2,1)}(-p_T) + \sqrt{\left( \mu_{(2,2,1)}(-p_T) - \frac{p_T}{2} \right)^2 + \tilde{M}_1^2} \right]^2 - \frac{p_T^2}{4} \right\}^{\frac{1}{2}}, \quad (4.28)$$

and the  $p_T$ -dependent parameter  $\mu_{(2,2,1)}(p_T)$  is defined in analogy to (4.13)

$$\mu_{(2,2,1)}(p_T) = \mu_{(2,2,1)} \left( \sqrt{1 + \left( \frac{p_T}{2M_2} \right)^2} - \frac{p_T}{2M_2} \right). \quad (4.29)$$

The size of the new kink  $\Delta\Theta^{(2,2,1)}$  can be easily read off from eq. (4.21), where one should make the obvious replacements  $M_0 \rightarrow M_1$  and  $M_1 \rightarrow M_2$ .

We can now generalize the two examples discussed so far ( $M_{T2}^{(1,1,0)}$  and  $M_{T2}^{(2,2,1)}$ ) to the case of an arbitrary grandparent index  $n$ , with  $p = n$  and  $c = n - 1$ . We get

$$M_{T2,max}^{(n,n,n-1)}(\tilde{M}_{n-1}, p_T) = \begin{cases} F_L^{(n,n,n-1)}(\tilde{M}_{n-1}, p_T), & \text{if } \tilde{M}_{n-1} \leq M_{n-1}, \\ F_R^{(n,n,n-1)}(\tilde{M}_{n-1}, p_T), & \text{if } \tilde{M}_{n-1} \geq M_{n-1}, \end{cases} \quad (4.30)$$

where

$$F_L^{(n,n,n-1)}(\tilde{M}_{n-1}, p_T) = \left\{ \left[ \mu_{(n,n,n-1)}(p_T) + \sqrt{\left( \mu_{(n,n,n-1)}(p_T) + \frac{p_T}{2} \right)^2 + \tilde{M}_{n-1}^2} \right]^2 - \frac{p_T^2}{4} \right\}^{\frac{1}{2}}, \quad (4.31)$$

$$F_R^{(n,n,n-1)}(\tilde{M}_{n-1}, p_T) = \left\{ \left[ \mu_{(n,n,n-1)}(-p_T) + \sqrt{\left( \mu_{(n,n,n-1)}(-p_T) - \frac{p_T}{2} \right)^2 + \tilde{M}_{n-1}^2} \right]^2 - \frac{p_T^2}{4} \right\}^{\frac{1}{2}}, \quad (4.32)$$

and the  $p_T$ -dependent parameter  $\mu_{(n,n,n-1)}(p_T)$  is simply the generalization of eqs. (4.13) and (4.29):

$$\mu_{(n,n,n-1)}(p_T) = \mu_{(n,n,n-1)} \left( \sqrt{1 + \left( \frac{p_T}{2M_n} \right)^2} - \frac{p_T}{2M_n} \right). \quad (4.33)$$

For  $n = 1$  or  $n = 2$ , the general formula (4.30) reproduces our previous results (4.10) and (4.26), correspondingly.

### 4.3 The subsystem variable $M_{T_2}^{(2,2,0)}$

The variable  $M_{T_2}^{(2,2,0)}$  is illustrated in Fig. 4(b), where we use the whole chain within the larger rectangle. As long as we ignore the effects of any ISR, we have a balanced<sup>6</sup> momentum configuration and the analytical results from Ref. [32] would apply. In particular, the endpoint  $M_{T_2, max}^{(2,2,0)}(\tilde{M}_0, p_T = 0)$  is given by [32]

$$M_{T_2, max}^{(2,2,0)}(\tilde{M}_0, p_T = 0) = \begin{cases} F_L^{(2,2,0)}(\tilde{M}_0, p_T = 0), & \text{if } \tilde{M}_0 \leq M_0, \\ F_R^{(2,2,0)}(\tilde{M}_0, p_T = 0), & \text{if } \tilde{M}_0 \geq M_0, \end{cases} \quad (4.34)$$

where

$$F_L^{(2,2,0)}(\tilde{M}_0, p_T = 0) = \mu_{(2,2,0)} + \sqrt{\mu_{(2,2,0)}^2 + \tilde{M}_0^2}, \quad (4.35)$$

$$F_R^{(2,2,0)}(\tilde{M}_0, p_T = 0) = \mu_{(2,2,1)} + \mu_{(2,1,0)} + \sqrt{(\mu_{(2,2,1)} - \mu_{(2,1,0)})^2 + \tilde{M}_0^2}, \quad (4.36)$$

and the various parameters  $\mu_{(n,p,c)}$  are defined in (4.1). Notice that these expressions are valid only for  $p_T = 0$ . We have also derived the corresponding generalized expression for  $M_{T_2, max}^{(2,2,0)}(\tilde{M}_0, p_T)$  for arbitrary values of  $p_T$ , which we list in Appendix A.

The most striking feature of the endpoint function (4.34) is that it will also exhibit a kink  $\Delta\Theta^{(2,2,0)}$  at the true value of the test mass  $\tilde{M}_0 = M_0$ . However, as emphasized in [31], the physical origin of this kink is different from the kinks  $\Delta\Theta^{(1,1,0)}$  and  $\Delta\Theta^{(2,2,1)}$  which we encountered previously in Secs. 4.1 and 4.2. This is easy to understand – in Secs. 4.1 and 4.2 we saw that the kinks  $\Delta\Theta^{(1,1,0)}$  and  $\Delta\Theta^{(2,2,1)}$  arise due to ISR effects, while eq. (4.34) holds in the absence of any ISR. The explanation for the  $\Delta\Theta^{(2,2,0)}$  kink has actually already been provided in [32]. In essence, one can treat the SM decay products  $x_1$  and  $x_2$  in each chain as a composite particle of variable mass, and the two branches  $F_L^{(2,2,0)}$  and  $F_R^{(2,2,0)}$  correspond to the two extreme values for the mass of this composite particle.

In spite of its different origin, the kink in the function (4.34) shares many of the same properties. Let us use a specific example as an illustration. Consider a popular example from supersymmetry, such as gluino pair-production, followed by sequential two-body decays to squarks and the lightest neutralinos. This is precisely a cascade of the type  $n = 2$ , in which  $X_2$  is the gluino  $\tilde{g}$ ,  $X_1$  is a squark  $\tilde{q}$ , and  $X_0$  is the lightest neutralino  $\tilde{\chi}_1^0$ . Let us choose the superpartner masses according to the SPS1a mass spectrum, which was also used in Ref. [32]:

$$M_2 = 613 \text{ GeV}, \quad M_1 = 525 \text{ GeV}, \quad M_0 = 99 \text{ GeV}. \quad (4.37)$$

The resulting function  $M_{T_2, max}^{(2,2,0)}(\tilde{M}_0, p_T = 0)$  is plotted in Fig. 6(a) with the upper set of lines (compare to Fig. 12(b) in Ref. [32]).

There are several noteworthy features of  $M_{T_2, max}^{(2,2,0)}(\tilde{M}_0, p_T = 0)$  which are evident from Fig. 6(a). First, when the test mass  $\tilde{M}_0$  is equal to the true child mass  $M_0$ , the  $M_{T_2}$  endpoint yields the true parent mass, in this case  $M_2$ :

$$M_{T_2, max}^{(2,2,0)}(\tilde{M}_0 = M_0, p_T = 0) = M_2. \quad (4.38)$$

---

<sup>6</sup>In the sense of eq. (4.8). See the discussion following eq. (4.8).



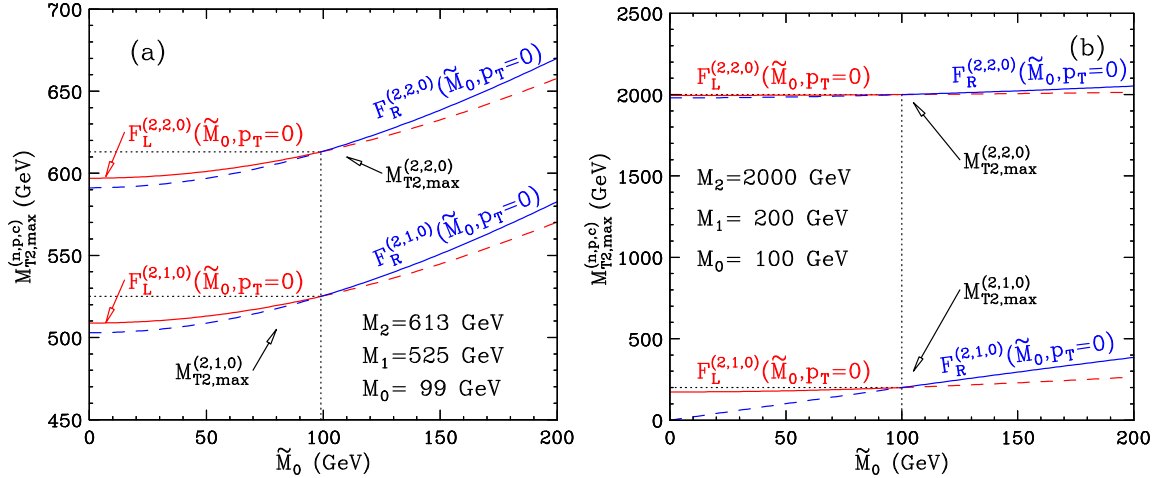


**Figure 6:** Dependence of the  $M_{T2,max}^{(2,2,0)}$  and  $M_{T2,max}^{(2,1,0)}$  upper kinematic endpoints on the value of the test mass  $\tilde{M}_0$ , for (a) the SPS1a parameter point in MSUGRA:  $M_2 = 613$  GeV,  $M_1 = 525$  GeV, and  $M_0 = 99$  GeV; or (b) a split spectrum  $M_2 = 2000$  GeV,  $M_1 = 200$  GeV, and  $M_0 = 100$  GeV. The horizontal (vertical) dotted lines denote the true value of the parent (child) mass for each case. Solid (dashed) lines indicate true (false) endpoints, while red (blue) lines correspond to  $F_L^{(n,p,c)}$  ( $F_R^{(n,p,c)}$ ) branches.

This property of  $M_{T2}$  is true by design, and is confirmed by the dotted lines in Fig. 6(a). Second, as seen from eq. (4.34),  $M_{T2,max}^{(2,2,0)}(\tilde{M}_0, p_T = 0)$  is not given by a single function, but has two separate branches. The first (“low”) branch  $F_L^{(2,2,0)}$  applies for  $\tilde{M}_0 \leq M_0$ , and is shown in Fig. 6(a) with red lines. The second (“high”) branch  $F_R^{(2,2,0)}$  is valid for  $\tilde{M}_0 \geq M_0$  and is shown in blue in Fig. 6(a). While the two branches coincide at  $\tilde{M}_0 = M_0$ :

$$F_L^{(2,2,0)}(M_0, p_T = 0) = F_R^{(2,2,0)}(M_0, p_T = 0) , \quad (4.39)$$

their *derivatives* do not match:

$$\left( \frac{\partial F_L^{(2,2,0)}}{\partial \tilde{M}_0} \right)_{\tilde{M}_0=M_0} \neq \left( \frac{\partial F_R^{(2,2,0)}}{\partial \tilde{M}_0} \right)_{\tilde{M}_0=M_0} , \quad (4.40)$$

leading to a kink  $\Delta\Theta^{(2,2,0)}$  in the function  $M_{T2,max}^{(2,2,0)}(\tilde{M}_0, p_T = 0)$  [29–32]. As before, let us try to investigate quantitatively the size of this kink. Applying the general definition (4.20), we obtain

$$\Delta\Theta^{(2,2,0)} = \arctan \left( \frac{2(1-y)(1-z)\sqrt{yz}}{(y+z)(1+yz) + 4yz} \right) , \quad (4.41)$$

where we have defined the squared mass ratios

$$y \equiv \frac{M_1^2}{M_2^2} , \quad z \equiv \frac{M_0^2}{M_1^2} . \quad (4.42)$$

The result (4.41) is plotted in Fig. 7(a) as a function of the mass ratios  $\sqrt{y}$  and  $\sqrt{z}$ . Fig. 7(a) demonstrates that as both  $y$  and  $z$  become small, the kink  $\Delta\Theta^{(2,2,0)}$  gets more pronounced.

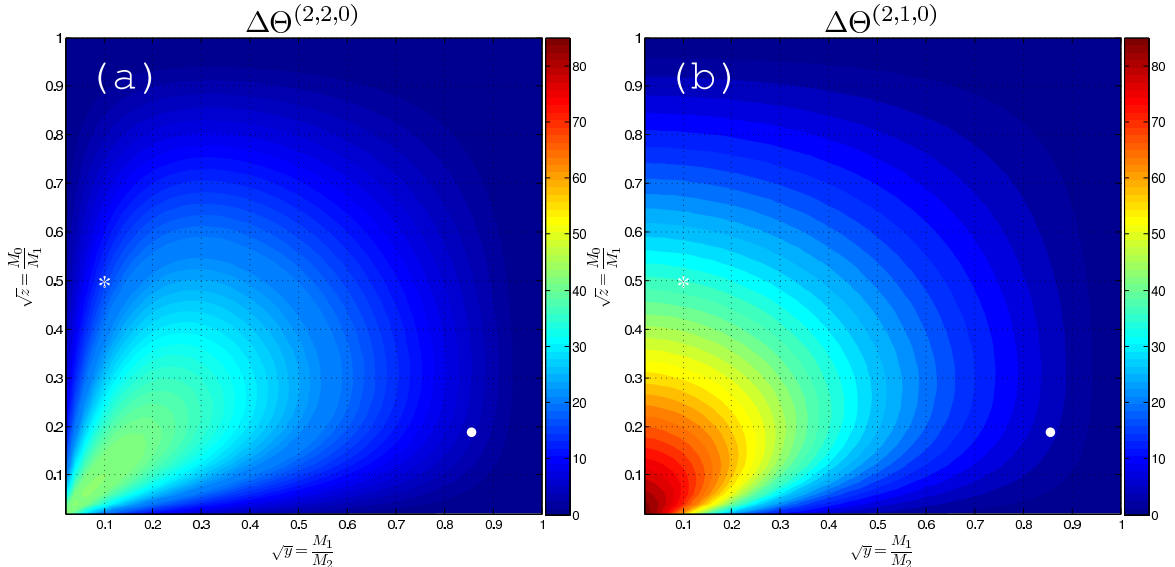


**Figure 7:** The amount of kink: (a)  $\Delta\Theta^{(2,2,0)}$  and (b)  $\Delta\Theta^{(2,1,0)}$  in degrees, as a function of the mass ratios  $\sqrt{y}$  and  $\sqrt{z}$ . The white dot and the white asterisk denote the locations in this  $(\sqrt{y}, \sqrt{z})$  parameter space of the two sample spectra (4.37) and (4.55) used for Figs. 6(a) and 6(b), correspondingly.

Fig. 7(a) also shows that the kink  $\Delta\Theta^{(2,2,0)}$  is a symmetric function of  $y$  and  $z$ , as can also be seen directly from eq. (4.41). Therefore, the kink  $\Delta\Theta^{(2,2,0)}$  will be best observable in those cases where  $y$  and  $z$  are both small, and in addition, the mass spectrum happens to obey the relation<sup>7</sup>  $y = z$ , i.e.  $M_1 = \sqrt{M_0 M_2}$ . Unfortunately, the SPS1a study point is rather far from this category – the spectrum (4.37) corresponds to the values  $\sqrt{y} = 0.856$  and  $\sqrt{z} = 0.189$ , which are indicated in Fig. 7(a) by a white dot. This conclusion is also supported by Fig. 6(a), which shows a rather mild kink in the SPS1a case.

We shall be rather ambivalent in our attitude toward the  $\Delta\Theta^{(2,2,0)}$  kink as well. While the interpretation of the kink is straightforward, its observation in the actual experiment is again an open issue. On the one hand, the experimental precision would depend on the particular signature, i.e. the type of the SM particles  $x_1$  and  $x_2$ . If those are leptons, their 4-momenta  $p_1^{(k)}$  and  $p_2^{(k)}$  will be measured relatively well and the kink might be observable. However, when  $x_1$  and  $x_2$  are jets, the experimental resolution may not be sufficient. Secondly, as seen in Fig. 6(a), the kink itself may not be very pronounced, and its observability will in fact depend on the particular mass spectrum.

The main lesson from the above discussion is that while the existence of the kink is without a doubt, its actual observation is by no means guaranteed. Therefore, our main mass measurement method, described later in Sec. 5.1, will not use any information related to the kink. In fact in Sec. 5.1 we shall show that one can completely reconstruct the mass spectrum of the new particles, using just measurements of  $M_{T2}$  endpoints, each done at a single fixed value of the corresponding test mass. It is worth noting that, in general, an endpoint in a spectrum is a sharper feature than a kink of the type (4.20). Therefore, we

<sup>7</sup>Notice that for this special value of  $M_1 = \sqrt{M_0 M_2}$ , the upper endpoint of the invariant mass distribution  $M_{x_1 x_2}$  is the same as in the case when the intermediate particle  $X_1$  is off-shell, i.e. when  $M_1 > M_2$ . Then we find that the  $M_{T2, max}^{(2,2,0)}$  formulas and corresponding kink structures are identical in the on-shell and off-shell cases. For details, see Appendix A.

would expect that the experimental precision on the extracted endpoints will be much better than the corresponding precision on the kink location. The kink will also not play any role in our hybrid method, described in Sec. 5.3. Only for the method described in Sec. 5.2, we shall try to make use of the kink information.

Let us now return to our original discussion of the  $M_{T_2}^{(2,2,0)}$  endpoint (4.34). Following our previous approach from Secs. 4.1 and 4.2, we would choose a fixed value of the test mass  $\tilde{M}_0$  and measure the corresponding  $M_{T_2}$  endpoint. However, the presence of two branches (4.35) and (4.36) leads to a slight complication: for a randomly chosen value of  $\tilde{M}_0$ , we will not know whether we should use (4.35) or (4.36) when interpreting the endpoint measurement. This requires us to make very special choices for the fixed value of  $\tilde{M}_0$ , which would remove this ambiguity. It is easy to see that by choosing  $\tilde{M}_0 = 0$ , we can ensure that the endpoint is always described by the “low” branch (4.35), and the  $M_{T_2,max}^{(2,2,0)}$  measurement can then be uniquely interpreted as

$$M_{T_2,max}^{(2,2,0)}(\tilde{M}_0 = 0, p_T = 0) = 2\mu_{(2,2,0)} = \frac{M_2^2 - M_0^2}{M_2}. \quad (4.43)$$

However, we could also design a special choice of  $\tilde{M}_0$ , which would select the “high” branch (4.35) and again uniquely remove the branch ambiguity. For this purpose, we must choose a value for the test mass  $\tilde{M}_0$  which is sufficiently large, in order to safely guarantee that it is well beyond the true mass  $M_0$ . Since the true mass  $M_0$  can never exceed the beam energy  $E_b$ , one obvious safe and rather conservative choice for  $\tilde{M}_0$  could be  $\tilde{M}_0 = E_b$ , in which case from (4.34) we get

$$\begin{aligned} M_{T_2,max}^{(2,2,0)}(\tilde{M}_0 = E_b, p_T = 0) &= \mu_{(2,2,1)} + \mu_{(2,1,0)} + \sqrt{(\mu_{(2,2,1)} - \mu_{(2,1,0)})^2 + E_b^2} \\ &= M_2 - \frac{M_2}{2} \left( \frac{M_1^2}{M_2^2} + \frac{M_0^2}{M_1^2} \right) + \sqrt{\frac{M_2^2}{4} \left( \frac{M_1^2}{M_2^2} - \frac{M_0^2}{M_1^2} \right)^2 + E_b^2}. \end{aligned} \quad (4.44)$$

Notice that the high branch function  $F_R^{(2,2,0)}$  in eq. (4.36) is rather unique in one very important aspect: it depends not just on one, but on *two* mass parameters, namely the combinations  $\mu_{(2,2,1)} + \mu_{(2,1,0)}$  and  $\mu_{(2,2,1)} - \mu_{(2,1,0)}$ . In contrast, the “low” branch  $F_L^{(2,2,0)}$ , as well as the previously discussed endpoint functions  $M_{T_2,max}^{(n,n,n-1)}(\tilde{M}_0, p_T = 0)$ , each contained a single  $\mu$  parameter. As a result, in those cases we did not benefit from any extra measurements for different values of the test mass  $\tilde{M}_0$  – had we done that, we would have been measuring the same  $\mu$  parameter over and over again. However, the situation with  $F_R^{(2,2,0)}$  is different, and here we *will* benefit from an additional measurement for a different value of  $\tilde{M}_0$ . For example, let us choose  $\tilde{M}_0 = E'_b$ , with  $E'_b > E_b$ , which will still keep us on the high branch. We obtain another constraint

$$\begin{aligned} M_{T_2,max}^{(2,2,0)}(\tilde{M}_0 = E'_b, p_T = 0) &= \mu_{(2,2,1)} + \mu_{(2,1,0)} + \sqrt{(\mu_{(2,2,1)} - \mu_{(2,1,0)})^2 + E_b'^2} \\ &= M_2 - \frac{M_2}{2} \left( \frac{M_1^2}{M_2^2} + \frac{M_0^2}{M_1^2} \right) + \sqrt{\frac{M_2^2}{4} \left( \frac{M_1^2}{M_2^2} - \frac{M_0^2}{M_1^2} \right)^2 + E_b'^2}. \end{aligned} \quad (4.45)$$

It is easy to check that the constraints (4.43-4.45) are all independent, thus providing *three* independent equations<sup>8</sup> for the three unknown masses  $M_0$ ,  $M_1$  and  $M_2$ . These three equations (4.43-4.45) can be solved rather easily<sup>9</sup>, and one obtains the proper solution for the masses  $M_0$ ,  $M_1$  and  $M_2$ , up to a two-fold ambiguity:

$$M_2 \rightarrow M_2, \quad M_1 \rightarrow \frac{M_0}{M_1} M_2, \quad M_0 \rightarrow M_0, \quad (4.46)$$

which is nothing but the interchange  $y \leftrightarrow z$  at a fixed  $M_2$ . The ambiguity arises because the expression (4.34) for the endpoint  $M_{T_2, max}^{(2,2,0)}$  (and consequently, the set of constraints (4.43-4.45)) is invariant under the transformation (4.46). Because of this ambiguity, in addition to the original SPS1a input values (4.37) for the mass spectrum, we obtain a second solution

$$M_2 = 613 \text{ GeV}, \quad M_1 = 115.6 \text{ GeV}, \quad M_0 = 99 \text{ GeV}. \quad (4.47)$$

This second solution was missed in the analysis of Ref. [32]. It is easy to check that the alternative mass spectrum (4.47) gives an identical  $M_{T_2, max}^{(2,2,0)}(\tilde{M}_0, p_T = 0)$  distribution as the one shown in Fig. 6(a), so that it is impossible to rule it out on the basis of  $M_{T_2, max}^{(2,2,0)}$  measurements alone.

The previous discussion reveals an important and somewhat overlooked benefit from the existence of the kink – one can make not one, not two, but *three* independent endpoint measurements from a single  $M_{T_2}^{(n,p,c)}$  distribution! In fact, we shall argue that the three measurements (4.43-4.45) are much more robust than the kink measurement (4.20). For example, when the child mass is relatively small, the lower branch  $F_L^{(2,2,0)}$  is relatively short and the kink will be difficult to see, even under ideal experimental conditions. An extreme example of this sort is presented in Section 5, where we discuss top quark events, in which the child (neutrino) mass  $M_0$  is practically zero and the kink cannot be seen at all. However, even under those circumstances, the endpoint measurements (4.43-4.45) are still available. More importantly, the constraints (4.43-4.45) are independent of the previously found relations (4.5) and (4.25), so that the latter can be used to resolve the two-fold ambiguity (4.46).

Before we move on to a discussion of the last remaining subsystem  $M_{T_2}$  quantity in the next Sec. 4.4, let us recap our main result derived in this subsection. We showed that the  $M_{T_2}^{(2,2,0)}$  variable yields *three* independent endpoint measurements (4.43-4.45), and possibly a kink measurement (4.20). The  $M_{T_2}^{(2,2,0)}$  endpoint measurements *by themselves* are sufficient to determine all three masses  $M_0$ ,  $M_1$  and  $M_2$ , up to the two-fold ambiguity (4.46). This represents a pure  $M_{T_2}$ -based mass measurement method, which does not use any any kink or invariant mass information.

---

<sup>8</sup>In practice, instead of relying on individual endpoint measurements for three different values of  $\tilde{M}_0$ , one may prefer to use the experimental information for the whole function  $M_{T_2, max}^{(2,2,0)}(\tilde{M}_0, p_T = 0)$  and simply fit to it the analytical expression (4.34) for the three floating parameters  $M_0$ ,  $M_1$  and  $M_2$ , as was done in Ref. [32]. As we shall see shortly, this method does not lead to any new information, and may only improve the statistical error on the mass determination. Therefore, to keep our discussion as simple as possible, we prefer to talk about the three individual measurements (4.43-4.45) as opposed to fitting the whole distribution (4.34).

<sup>9</sup>The general solution for  $M_2$ ,  $M_1$  and  $M_0$  in terms of the measured endpoints (4.43-4.45) is rather messy and not very illuminating, therefore we do not list it here.

#### 4.4 The subsystem variable $M_{T_2}^{(2,1,0)}$

The variable  $M_{T_2}^{(2,1,0)}$  is illustrated in Fig. 4(b), where we use the subchain within the smaller rectangle on the right. This is another genuine subsystem quantity, since we only use the SM decay products  $x_1$  and ignore the upstream objects  $x_2$ . However, the upstream objects  $x_2$  are important in the sense that they have some non-zero transverse momentum, and as a result, the sum of the transverse momenta  $\vec{P}_{0T}^{(k)}$  of the children  $X_0$  is *not* balanced by the sum of the transverse momenta of the SM objects  $x_1$  used in the  $M_{T_2}$  calculation:

$$\vec{P}_{0T}^{(1)} + \vec{P}_{0T}^{(2)} + \vec{p}_{1T}^{(1)} + \vec{p}_{1T}^{(2)} = -\vec{p}_{2T}^{(1)} - \vec{p}_{2T}^{(2)} - \vec{p}_T \neq 0. \quad (4.48)$$

Notice that even in the absence of any ISR  $p_T$ , this is still an unbalanced configuration, due to the transverse momenta  $\vec{p}_{2T}^{(1)}$  and  $\vec{p}_{2T}^{(2)}$  of the upstream objects  $x_2$ . Therefore, we cannot use the existing analytical results on  $M_{T_2}$ , since previous studies always assumed that the right-hand side of eq. (4.48) is exactly zero, due to the lack of any particles upstream. We therefore need to generalize the previous treatments of  $M_{T_2}$  and obtain the corresponding endpoint formulas for our new subsystem  $M_{T_2}^{(2,1,0)}$  variable. The general mathematical properties of subsystem  $M_{T_2}^{(n,p,c)}$  variables will be presented in a forthcoming publication [49]. Here we shall only use the results relevant for our example ( $n = 2$ ). In particular, in the absence of any intrinsic ISR (i.e., for  $p_T = 0$ ), we find that the endpoint of the  $M_{T_2}^{(2,1,0)}$  distribution is given by

$$M_{T_2,max}^{(2,1,0)}(\tilde{M}_0, p_T = 0) = \begin{cases} F_L^{(2,1,0)}(\tilde{M}_0, p_T = 0), & \text{if } \tilde{M}_0 \leq M_0, \\ F_R^{(2,1,0)}(\tilde{M}_0, p_T = 0), & \text{if } \tilde{M}_0 \geq M_0, \end{cases} \quad (4.49)$$

where

$$F_L^{(2,1,0)}(\tilde{M}_0, p_T = 0) = \left\{ \left[ \mu_{(2,2,0)} - \mu_{(2,2,1)} + \sqrt{\mu_{(2,2,0)}^2 + \tilde{M}_0^2} \right]^2 - \mu_{(2,2,1)}^2 \right\}^{\frac{1}{2}}, \quad (4.50)$$

$$F_R^{(2,1,0)}(\tilde{M}_0, p_T = 0) = \left\{ \left[ \mu_{(2,1,0)} + \sqrt{(\mu_{(2,2,1)} - \mu_{(2,1,0)})^2 + \tilde{M}_0^2} \right]^2 - \mu_{(2,2,1)}^2 \right\}^{\frac{1}{2}}, \quad (4.51)$$

and the various parameters  $\mu_{(n,p,c)}$  are defined in (4.1). The corresponding expressions for general  $p_T$  (i.e., arbitrary intrinsic ISR) are listed in Appendix A.

From eq. (4.49) we see that, once again, the endpoint function  $M_{T_2,max}^{(2,1,0)}(\tilde{M}_0, p_T = 0)$  would exhibit a kink  $\Delta\Theta^{(2,1,0)}$  at the true value of the test mass  $\tilde{M}_0 = M_0$ :

$$\left( \frac{\partial F_L^{(2,1,0)}}{\partial \tilde{M}_0} \right)_{\tilde{M}_0=M_0} \neq \left( \frac{\partial F_R^{(2,1,0)}}{\partial \tilde{M}_0} \right)_{\tilde{M}_0=M_0}. \quad (4.52)$$

The existence of this kink should come as no surprise — Ref. [31] showed (in the  $p_T \rightarrow \infty$  limit) that *any* type of upstream momentum will generate a kink in an otherwise smooth  $M_{T_2,max}^{(2,1,0)}$  function. As before, the value of the  $M_{T_2}$  endpoint  $M_{T_2,max}^{(2,1,0)}$  at the kink location reveals the true mass of the parent:

$$M_{T_2,max}^{(2,1,0)}(\tilde{M}_0 = M_0, p_T = 0) = M_1. \quad (4.53)$$

At the same time, the physical origin of this kink is different from either of the two kink types ( $\Delta\Theta^{(1,1,0)}$  and  $\Delta\Theta^{(2,2,0)}$ ) discussed earlier. Clearly, the new kink is different from  $\Delta\Theta^{(2,2,0)}$ , which was due to the varying invariant mass of the  $\{x_1, x_2\}$  system. Here we are using a single SM particle  $x_1$  whose mass is constant. Furthermore, the new kink  $\Delta\Theta^{(2,1,0)}$  cannot be due to any ISR like in the case of  $\Delta\Theta^{(1,1,0)}$ , since eq. (4.49) does not account for any ISR effects. The real reason for this new  $\Delta\Theta^{(2,1,0)}$  kink is a third one, namely, the kinematical restrictions placed by the decays of the upstream particles (in this case, the grandparents  $X_2$ ).

We now proceed to investigate the new kink  $\Delta\Theta^{(2,1,0)}$  quantitatively. Using the same example of gluino pair-production for the SPS1a mass spectrum (4.37), we plot the function (4.49) in Fig. 6(a). Comparing the lower and the upper set of lines in the figure, we notice that the  $M_{T2,max}^{(2,1,0)}$  and  $M_{T2,max}^{(2,2,0)}$  variables share several common characteristics. They both exhibit a kink at the true location of the child mass  $\tilde{M}_0 = M_0$ , while their values at that point reveal the true parent mass in each case:  $M_1$  for  $M_{T2,max}^{(2,1,0)}$  and  $M_2$  for  $M_{T2,max}^{(2,2,0)}$ . Using the definition (4.20), we find that the size of the  $\Delta\Theta^{(2,1,0)}$  kink is given by

$$\Delta\Theta^{(2,1,0)} = \arctan\left(\frac{(1-y^2)(1-z)\sqrt{z}}{2z(1+y^2)+y(1+z^2)+2yz}\right), \quad (4.54)$$

where the parameters  $y$  and  $z$  were already defined in (4.42). The kink  $\Delta\Theta^{(2,1,0)}$  is plotted in Fig. 7(b) as a function of  $\sqrt{y}$  and  $\sqrt{z}$ . We notice that the kink structure becomes more pronounced for relatively small  $y$  and  $z$ . Comparing Figs. 7(a) and 7(b), we see that for any given set of values for  $y$  and  $z$ , the  $\Delta\Theta^{(2,1,0)}$  kink discussed here is more pronounced than the  $\Delta\Theta^{(2,2,0)}$  kink from the previous subsection<sup>10</sup>. The difference is particularly noticeable in the region of  $\sqrt{y} \sim 0$  and  $\sqrt{z} \sim 0.2$ . The SPS1a mass spectrum (4.37) in our previous example was rather far away from this region, as indicated by the white dots in Fig. 7. Now let us choose a different mass spectrum, which is closer to the region where the difference between the two kinks becomes more noticeable, for example

$$M_2 = 2000 \text{ GeV}, \quad M_1 = 200 \text{ GeV}, \quad M_0 = 100 \text{ GeV}, \quad (4.55)$$

corresponding to the point marked with the white asterisk in Figs. 7(a) and 7(b). The resulting endpoint functions  $M_{T2,max}^{(2,2,0)}$  and  $M_{T2,max}^{(2,1,0)}$  are plotted in Fig. 6(b). Indeed we see that with this new spectrum the kink in the  $M_{T2,max}^{(2,1,0)}$  function is much more noticeable than the kink in the  $M_{T2,max}^{(2,2,0)}$  function. Therefore, our first conclusion regarding the  $M_{T2}^{(2,1,0)}$  variable is that its kink is in general sharper and appears to be more promising than the previously discussed kink in the  $M_{T2}^{(2,2,0)}$  variable from Sec. 4.3.

Following our previous strategy, we shall not dwell too long on the kink, but instead we shall discuss the available endpoint measurements for various values of  $\tilde{M}_0$ . Again, the presence of two branches in eq. (4.49) can be used to our advantage. As in Sec. 4.3, we first choose a test mass value  $\tilde{M}_0 = 0$ , which would “select” the low branch (4.50) and result in

---

<sup>10</sup>This statement can also be verified using the analytical formulas (4.41) and (4.54).

an endpoint measurement

$$M_{T2,max}^{(2,1,0)}(\tilde{M}_0 = 0, p_T = 0) = 2 \sqrt{\mu_{(2,2,0)} (\mu_{(2,2,0)} - \mu_{(2,2,1)})}. \quad (4.56)$$

Just as before, we could also choose a rather large value for  $\tilde{M}_0 = E_b$ , which would select the high branch (4.51) and result in the measurement

$$M_{T2,max}^{(2,1,0)}(\tilde{M}_0 = E_b, p_T = 0) = \left\{ \left[ \mu_{(2,1,0)} + \sqrt{(\mu_{(2,2,1)} - \mu_{(2,1,0)})^2 + E_b^2} \right]^2 - \mu_{(2,2,1)}^2 \right\}^{\frac{1}{2}}. \quad (4.57)$$

A third choice,  $\tilde{M}_0 = E'_b$ , with  $E'_b > E_b$ , would yield yet another endpoint measurement

$$M_{T2,max}^{(2,1,0)}(\tilde{M}_0 = E'_b, p_T = 0) = \left\{ \left[ \mu_{(2,1,0)} + \sqrt{(\mu_{(2,2,1)} - \mu_{(2,1,0)})^2 + E'^2_b} \right]^2 - \mu_{(2,2,1)}^2 \right\}^{\frac{1}{2}}. \quad (4.58)$$

Again we obtained three equations (4.56-4.58) for the three unknown  $\mu$ -parameters  $\mu_{(2,2,0)}$ ,  $\mu_{(2,2,1)}$  and  $\mu_{(2,1,0)}$ , or equivalently, for the three unknown masses  $M_0$ ,  $M_1$  and  $M_2$ . These equations are all independent and can be easily solved, giving a total of four solutions. However, three of the solutions are always unphysical, so that we end up with a single unique solution. This represents an important advantage of the  $M_{T2,max}^{(2,1,0)}$  variable in comparison with the  $M_{T2,max}^{(2,2,0)}$  variable discussed in Sec. 4.3. There we found that  $M_{T2,max}^{(2,2,0)}$  always gives rise to a two-fold ambiguity in the mass spectrum, while now we see that  $M_{T2,max}^{(2,1,0)}$  does not suffer from this problem and already by itself allows for a complete and unambiguous determination of the mass spectrum.

## 5. $M_{T2}$ -based mass measurement methods

In this section we use the analytical results derived in the previous section to propose three different strategies for determining the masses in  $n \leq 2$  decay chains. We shall illustrate each of our methods with a specific example, for which we choose to consider the dilepton samples from  $W^+W^-$  and  $t\bar{t}$  events. The former is an example of the  $n = 1$  decay chain exhibited in Fig. 4(a), while the latter is an example of the  $n = 2$  decay chain in Fig. 4(b). Most importantly, these samples already exist in the Tevatron data and will also be among the first to be studied at the LHC. Correspondingly, throughout this section we shall use the following mass spectrum

$$\begin{aligned} M_2 &= m_t = 173 \text{ GeV}, \\ M_1 &= m_W = 80 \text{ GeV}, \\ M_0 &= m_\nu = 0 \text{ GeV}. \end{aligned} \quad (5.1)$$

Before we begin, let us review the four different  $M_{T2}^{(n,p,c)}$  variables which are in principle available in that case. Each one of them is plotted in Fig. 8 for five different values of the

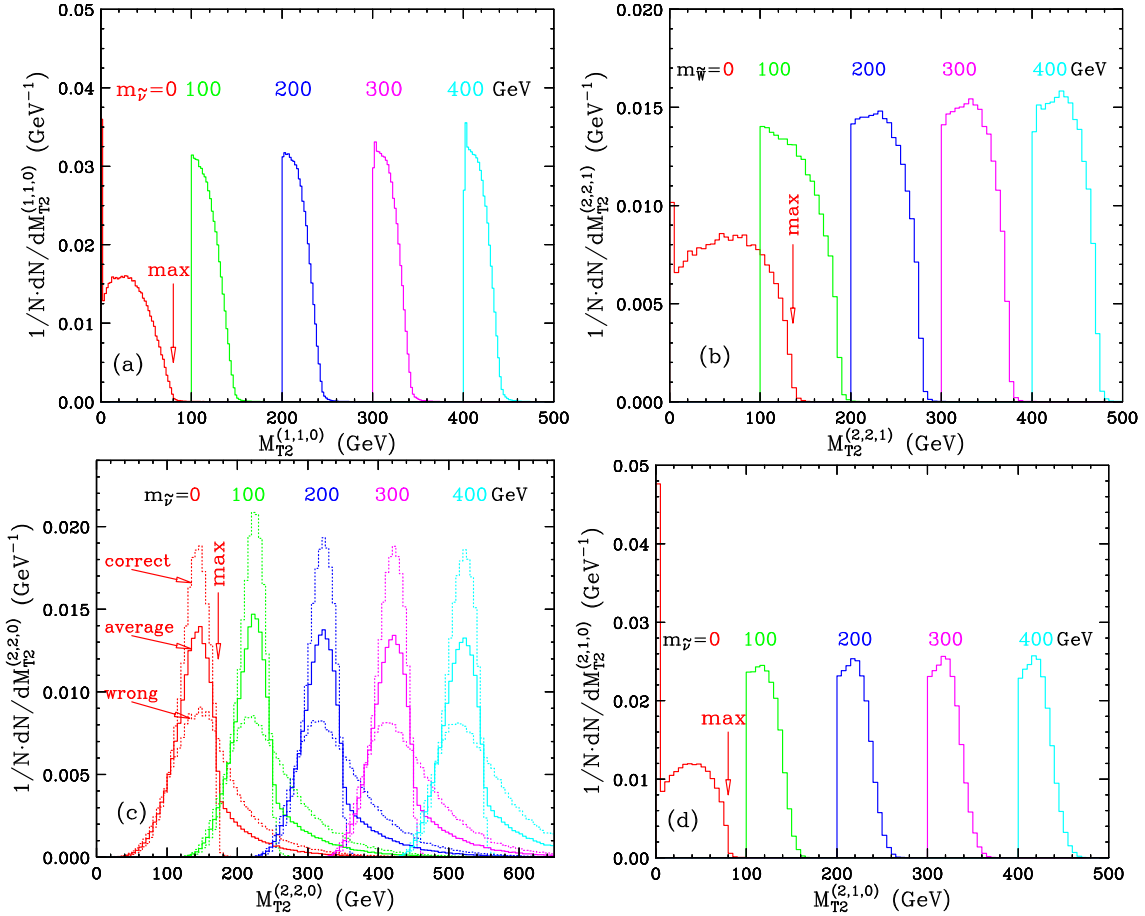


**Figure 8:** Unit-normalized distributions of  $M_{T2}^{(n,p,c)}$  variables in dilepton events from (a)  $W^+W^-$  pair production and (b-d)  $t\bar{t}$  pair production. Each panel shows results for five different values (0, 100, 200, 300 and 400 GeV) of the corresponding test mass. The methods of Secs. 5.1 and 5.3 only make use of the  $M_{T2}$  endpoint at zero test mass,  $M_{T2,max}^{(n,p,c)}(\tilde{M}_c = 0)$ , which is indicated by the vertical red arrow. In panel (c), the two dotted line  $M_{T2}^{(2,2,0)}$  distributions correspond to the correct and the wrong pairing of the two  $b$ -jets with the leptons, while the solid line distribution is the average of these two.

corresponding test mass (0, 100, 200, 300 and 400 GeV). In Fig. 8(a) we show the  $M_{T2}^{(1,1,0)}$  variable from  $W^+W^-$  pair production events, while in Figs. 8(b-d) we correspondingly show the  $M_{T2}^{(2,2,1)}$ ,  $M_{T2}^{(2,2,0)}$  and  $M_{T2}^{(2,1,0)}$  variables from  $t\bar{t}$  events. We used PYTHIA for event generation and did not impose any selection cuts, since they will not affect the location of the  $M_{T2}$  endpoint<sup>11</sup>. The plots are made for the Tevatron (a  $p\bar{p}$  collider with a 2 TeV center-of-mass energy), where the relevant data is already available. The corresponding analysis for the LHC is very similar. All of our plots in this Section have the full ISR effects. As discussed in Section 4, the presence of ISR with nonzero  $p_T$  will increase the nominal  $M_{T2}^{(n,p,c)}$

<sup>11</sup>The cuts would have an impact on the overall acceptance and efficiency. This effect is not relevant here, since we are showing unit-normalized distributions. The cuts may also distort the shape of each distribution, but should preserve the location of the upper endpoint.



endpoints:

$$M_{T2,max}^{(n,p,c)}(\tilde{M}_c, p_T) \geq M_{T2,max}^{(n,p,c)}(\tilde{M}_c, 0), \quad (5.2)$$

where the equality is obtained only when  $\tilde{M}_c = M_c$ . ISR will therefore introduce some systematic error when one is trying to measure  $M_{T2,max}^{(n,p,c)}(\tilde{M}_c, 0)$ . The size of this error depends on the ISR  $p_T$  spectrum, which in turn depends on the type of collider (Tevatron or LHC). At the Tevatron, this will not be such a serious issue, as evidenced from Fig. 8, where the observed endpoints in the presence of ISR match pretty well with their expected values for the  $p_T = 0$  case. On the other hand, at the LHC this may become a problem, which can be handled in one of two ways. First, depending on the particular signature, one may be able to select a sample with  $p_T \approx 0$  (at a certain cost in statistics), by imposing a suitably designed jet veto to remove jets from ISR. Alternatively, one can use the full event sample (which would include ISR jets), and make use of our general formulas in Appendix A, which contain the explicit  $p_T$  dependence of  $M_{T2,max}^{(n,p,c)}$ .

In the previous Section 4 we derived that in the case of  $n \leq 2$  cascades, there are 8 different  $M_{T2}$  endpoint measurements: one for  $M_{T2,max}^{(1,1,0)}$  (see eq. (4.5) and Sec. 4.1), one for  $M_{T2,max}^{(2,2,1)}$  (see eq. (4.25) and Sec. 4.2), three for  $M_{T2,max}^{(2,2,0)}$  (see eqs. (4.43-4.45) and Sec. 4.3), and three for  $M_{T2,max}^{(2,1,0)}$  (see eqs. (4.56-4.58) and Sec. 4.4). Given that we are trying to determine only three masses  $M_0$ ,  $M_1$  and  $M_2$ , it is clear that these 8 measurements should be sufficient to completely determine the spectrum. We also see that our previous count (3.8) has actually greatly underestimated the power of  $M_{T2}$ , and the number of available measurements is in fact much larger than the number of  $M_{T2,max}^{(n,p,c)}$  variables. Indeed, as shown in Sections 4.3 and 4.4, there are cases where we might be able to obtain more than one mass constraint from a given  $M_{T2,max}^{(n,p,c)}$  variable. Of course, the 8 measurements cannot all be independent among themselves, as they only depend on three parameters. Our three methods below will be distinguished based on which subset of these measurements we are using.

### 5.1 Pure $M_{T2}$ endpoint method

With this method, we use  $M_{T2}$  endpoint measurements  $E_{npc}$  at a single fixed value of the test mass, which for convenience we take to be  $\tilde{M}_c = 0$ :

$$E_{npc} \equiv M_{T2,max}^{(n,p,c)}(\tilde{M}_c = 0, p_T = 0). \quad (5.3)$$

The corresponding formulas interpreting those measurements in terms of the physical masses  $M_0$ ,  $M_1$  and  $M_2$  were derived in Sec. 4:

$$E_{110} \equiv M_{T2,max}^{(1,1,0)}(0, 0) = \frac{M_1^2 - M_0^2}{M_1} = M_2 \sqrt{y} (1 - z), \quad (5.4)$$

$$E_{221} \equiv M_{T2,max}^{(2,2,1)}(0, 0) = \frac{M_2^2 - M_1^2}{M_2} = M_2 (1 - y), \quad (5.5)$$

$$E_{220} \equiv M_{T2,max}^{(2,2,0)}(0, 0) = \frac{M_2^2 - M_0^2}{M_2} = M_2 (1 - yz), \quad (5.6)$$

$$E_{210} \equiv M_{T2,max}^{(2,1,0)}(0, 0) = \frac{1}{M_2} \sqrt{(M_2^2 - M_0^2)(M_1^2 - M_0^2)} = M_2 \sqrt{y(1-z)(1-yz)}. \quad (5.7)$$

Using the mass spectrum (5.1), the predicted locations of these four  $M_{T_2}$  endpoints are

$$E_{110} = 80 \text{ GeV} , \quad (5.8)$$

$$E_{221} = 136 \text{ GeV} , \quad (5.9)$$

$$E_{220} = 173 \text{ GeV} , \quad (5.10)$$

$$E_{210} = 80 \text{ GeV} , \quad (5.11)$$

which are marked with the vertical red arrows in Fig. 8. Given that we have four measurements (5.4-5.7) for only three parameters  $M_0$ ,  $M_1$  and  $M_2$ , one should be able to uniquely determine all three of the unknown parameters. Naively, it seems that using just three of the measurements (5.4-5.7) should be sufficient for this purpose, and furthermore, that *any* three of the measurements (5.4-5.7) will do the job. However, one should exercise caution, since not all four measurements (5.4-5.7) are independent. It is easy to check that  $E_{221}$ ,  $E_{220}$  and  $E_{210}$  obey the following relation

$$E_{210}^2 = E_{220} (E_{220} - E_{221}) . \quad (5.12)$$

This means that in order to be able to solve for the masses from eqs. (5.4-5.7), we must always make use of the  $E_{110}$  measurement in eq. (5.4), and then we have the freedom to choose any two out of the remaining three measurements (5.5-5.7). For example, using the set of three measurements  $\{E_{110}, E_{221}, E_{220}\}$  (i.e. eqs. (5.4-5.6)), the masses are uniquely determined as

$$M_0 = \frac{E_{110} \{E_{221}(E_{220} - E_{221}) [E_{220}(E_{220} - E_{221}) - E_{110}^2]\}^{\frac{1}{2}}}{E_{110}^2 - (E_{220} - E_{221})^2} , \quad (5.13)$$

$$M_1 = \frac{E_{110} E_{221} (E_{220} - E_{221})}{E_{110}^2 - (E_{220} - E_{221})^2} , \quad (5.14)$$

$$M_2 = \frac{E_{110}^2 E_{221}}{E_{110}^2 - (E_{220} - E_{221})^2} . \quad (5.15)$$

Similarly, one can solve for  $M_0$ ,  $M_1$  and  $M_2$  using the set of measurements  $\{E_{110}, E_{220}, E_{210}\}$ , or alternatively, the set of measurements  $\{E_{110}, E_{221}, E_{210}\}$ . In each case, the remaining fourth unused measurement provides a useful consistency check on the mass determination.

## 5.2 $M_{T_2}$ endpoint shapes and kinks

The method proposed in Sec. 5.1 uses the measured endpoints from *several different*  $M_{T_2}^{(n,p,c)}$  variables. Now we discuss an alternative method which makes use of *a single*  $M_{T_2}^{(n,p,c)}$  variable.

Let us begin with the simplest case of  $n = 1$  as shown in Fig. 4(a). In that case, we have only one  $M_{T_2}$  variable at our disposal, namely  $M_{T_2}^{(1,1,0)}$ . Its properties were discussed in Sec. 4.1, where we showed that its endpoint  $M_{T_2, \max}^{(1,1,0)}$  can allow the determination of *both* masses  $M_0$  and  $M_1$ , at least as a matter of principle. Indeed, the endpoint measurement (5.4) at zero test mass provides one relation among  $M_0$  and  $M_1$ . The key observation in Sec. 4.1 (which was first done in [31]) was that with the inclusion of ISR effects, the endpoint

function  $M_{T2,max}^{(1,1,0)}(\tilde{M}_0, p_T)$  exhibits a kink at  $\tilde{M}_0 = M_0$ , which can then be used to determine both masses  $M_0$  and  $M_1$ . The method can be readily applied to the existing dilepton event sample from  $W^+W^-$  pair production, which will allow an independent measurement of the  $W$  mass  $m_W$  and the neutrino mass  $m_\nu$ . While the precision of this measurement will not be competitive with existing  $W$  and neutrino mass determinations, it is nevertheless useful to test the viability of this approach with real data.

Now let us discuss the more complicated case of  $n = 2$ , which in our example corresponds to  $t\bar{t}$  pair production with both tops decaying leptonically. As discussed in Secs. 4.2, 4.3 and 4.4, here we have a choice of three different  $M_{T2}$  variables:  $M_{T2}^{(2,2,1)}$ ,  $M_{T2}^{(2,2,0)}$ , and  $M_{T2}^{(2,1,0)}$ . Because of the larger  $t\bar{t}$  cross-section, we expect that the statistical precision on each one of those three variables will be better than the  $M_{T2}^{(1,1,0)}$  variable of the  $n = 1$  case. As shown in Secs. 4.3 and 4.4, each of the two variables  $M_{T2}^{(2,2,0)}$  and  $M_{T2}^{(2,1,0)}$  exhibits a kink in its endpoint  $M_{T2,max}^{(n,p,c)}$  when considered as a function of the test mass  $\tilde{M}_0$ , even when the transverse momentum of the intrinsic ISR in the event is zero,  $p_T = 0$ . Then, which of these two variables is better suited for a mass determination? The case of  $M_{T2,max}^{(2,2,0)}(\tilde{M}_0, p_T = 0)$  was already discussed in [29, 31, 32]. Here we would like to propose the alternative measurement of  $M_{T2,max}^{(2,1,0)}(\tilde{M}_0, p_T = 0)$ . What is more, we would like to emphasize that our function  $M_{T2,max}^{(2,1,0)}(\tilde{M}_0, p_T = 0)$  offers several unique advantages over the previously considered case of  $M_{T2,max}^{(2,2,0)}(\tilde{M}_0, p_T = 0)$ :

1. The subsystem variable  $M_{T2}^{(2,1,0)}$  does not suffer from the combinatorics problem which is present for  $M_{T2}^{(2,2,0)}$ . Indeed, when constructing the  $M_{T2}^{(2,2,0)}$  distribution, one has to decide how to pair up the  $b$ -jets with the two leptons. Because it is difficult to distinguish between a  $b$  and a  $\bar{b}$ , there is a two-fold ambiguity which is quite difficult to resolve by other means. In contrast, our subsystem variable  $M_{T2}^{(2,1,0)}$  does not make direct use of the  $b$ -jets, and is therefore free of such combinatorics issues.
2. As we already saw in Sec. 4.3, even under perfect experimental conditions, the fit to the  $M_{T2,max}^{(2,2,0)}$  endpoint results in two separate solutions for the mass spectrum: one solution (see (4.37)) is given by the true values of the input masses, while the second solution (see (4.47)) is obtained by the transformation (4.46). Using  $M_{T2,max}^{(2,2,0)}$  alone, there is no way to tell the difference between these two mass spectra. In contrast, our variable  $M_{T2}^{(2,1,0)}$  does not suffer from this ambiguity, and according to our results from Sec. 4.4 the solution is always unique.
3. The third advantage of the subsystem variable  $M_{T2}^{(2,1,0)}$  is related to the expected precision on the determination of the masses. As we pointed out in Sec. 4.4 and illustrated explicitly in Fig. 7, the kink  $\Delta\Theta^{(2,1,0)}$  in the  $M_{T2,max}^{(2,1,0)}(\tilde{M}_0, p_T = 0)$  function is much sharper than the corresponding kink  $\Delta\Theta^{(2,2,0)}$  in the  $M_{T2,max}^{(2,2,0)}(\tilde{M}_0, p_T = 0)$  function. This can also be seen explicitly from the two examples shown in Fig. 6. As a result, we expect that the kink structure can be better identified in the case of  $M_{T2,max}^{(2,1,0)}$ , which would lead to smaller errors on the mass determination.

Of course, one could (and in fact should) use the experimental information from *both*  $M_{T_2,max}^{(2,2,0)}$  and  $M_{T_2,max}^{(2,1,0)}$ , if available. Our main goal here is simply to point out the obvious advantages of the subsystem variable  $M_{T_2}^{(2,1,0)}$ , which so far has not been used in the literature.

### 5.3 Hybrid method: $M_{T_2}$ endpoints plus an invariant mass endpoint

As discussed in Sec. 2.1, any cascade with  $n \geq 2$  will provide a certain number of measurements (2.5) in addition to the  $M_{T_2}$  measurements discussed so far. In particular, for the  $n = 2$  example considered here, there will be one measurement of the endpoint of the  $M_{x_1x_2}$  invariant mass distribution. The formula for the endpoint  $M_{x_1x_2,max}$  in terms of the unknown physical masses  $M_0$ ,  $M_1$  and  $M_2$  is in general given by

$$E_{im} \equiv M_{x_1x_2,max} = \frac{1}{M_1} \sqrt{(M_2^2 - M_1^2)(M_1^2 - M_0^2)} = M_2 \sqrt{(1-y)(1-z)}. \quad (5.16)$$

In the case of  $t\bar{t}$  events considered here, this is simply the endpoint of the invariant mass distribution  $m_{b\ell}$  of each lepton and its corresponding  $b$ -jet. This distribution (unit-normalized) is shown in Fig. 9. Unfortunately, here one is facing the same combinatorial problem as with the  $M_{T_2}^{(2,2,0)}$  variable – we cannot easily tell the charge of the  $b$ -jet, therefore a priori it is not clear which  $b$ -jet goes with which lepton. Fortunately, there are only two possibilities: the result from the correct (wrong) pairing is shown in Fig. 9 with the green (blue) dotted line. We see that the green histogram with the correct pairing has an endpoint at the expected location

$$E_{im} = \sqrt{\frac{(m_t^2 - m_W^2)(m_W^2 - m_\nu^2)}{m_W^2}} = 153.4 \text{ GeV}, \quad (5.17)$$

with a relatively small tail due to the finite width effects. More importantly, the (blue) distribution from the wrong pairings is relatively smooth, and as a result the endpoint (5.17) is preserved in the experimentally observable (red) distribution, which includes all possible  $b\ell$  pairings.

Now we can add the new measurement (5.16) to the previously discussed set of measurements (5.4-5.7). We obtain a total of five measurements for the three underlying parameters  $M_0$ ,  $M_1$  and  $M_2$ , therefore there exist two relations among the measurements. The first relation is already given by (5.12) and does not involve the invariant mass endpoint (5.16). The second relation is given by

$$E_{im}^2 = \frac{E_{221}E_{110}^2}{E_{220} - E_{221}}. \quad (5.18)$$

We can now consider a hybrid method, which would make use of the invariant mass endpoint (5.16), plus any two of the  $M_{T_2}$  measurements (5.4-5.7). In principle, one again needs to be careful and make sure that the three used measurements are independent. Fortunately, as seen from eqs. (5.12,5.18), the invariant mass endpoint  $E_{im}$  is independent from *any* pair of  $M_{T_2}$  measurements. There are 6 possible pairs among the  $M_{T_2}$  measurements (5.4-5.7), and in principle each one can be used in combination with the invariant mass endpoint (5.16). What is the best choice? We find that in all 6 of those cases one obtains a unique solution for

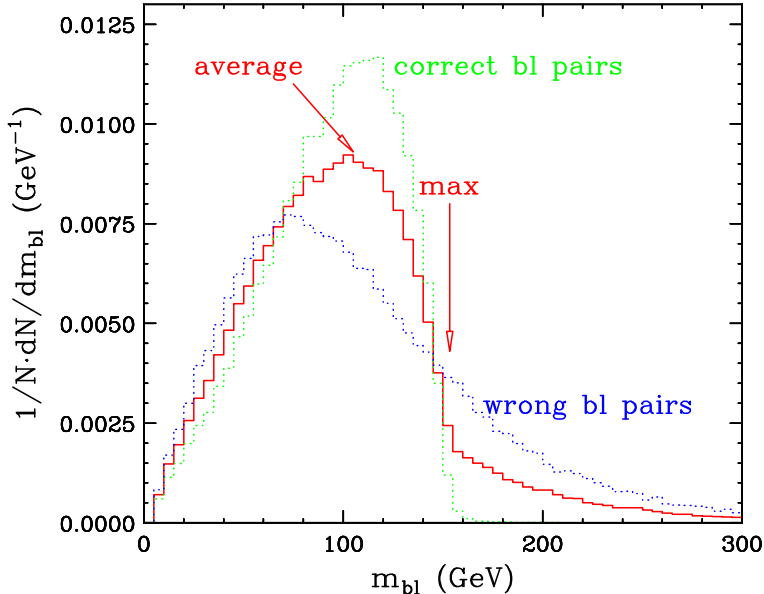


**Figure 9:** Unit-normalized  $m_{b\ell}$  invariant mass-squared distributions in dilepton  $t\bar{t}$  events. The green (blue) dotted line corresponds to the correct (wrong) pairing of the leptons and the  $b$ -jets, while the red solid line is the average of those two distributions. The endpoint (5.16) of the  $m_{b\ell}$  distribution is marked by the vertical red arrow.

the masses  $M_0$ ,  $M_1$  and  $M_2$ . Therefore, the optimal choice is dictated by the experimental precision on each of the measurements (5.4-5.7). We expect that the measurement (4.3) of  $M_{T_2,max}^{(1,1,0)}$  will be less precise due to the smaller cross-section for  $W^+W^-$  production. Similarly,  $M_{T_2,max}^{(2,2,0)}$  suffers from the combinatorial problem already mentioned earlier. Therefore for our illustration of the hybrid method we choose to use the  $M_{T_2}^{(2,2,1)}$  endpoint (5.5), the  $M_{T_2}^{(2,1,0)}$  endpoint (5.7), and the invariant mass endpoint (5.16). The solution for the masses in terms of those three measurements is given by

$$M_0 = \frac{\sqrt{2E_{221}} E_{im} \left( 2E_{221} E_{210}^2 + E_{221} E_{im}^2 - E_{im}^2 \sqrt{E_{221}^2 + 4E_{210}^2} \right)^{\frac{1}{2}}}{E_{221}^2 + 2E_{im}^2 - E_{221} \sqrt{E_{221}^2 + 4E_{210}^2}}, \quad (5.19)$$

$$M_1 = \frac{\sqrt{2} E_{221} E_{im} \left( E_{221} \sqrt{E_{221}^2 + 4E_{210}^2} - E_{221}^2 \right)^{\frac{1}{2}}}{E_{221}^2 + 2E_{im}^2 - E_{221} \sqrt{E_{221}^2 + 4E_{210}^2}}, \quad (5.20)$$

$$M_2 = \frac{2E_{221} E_{im}^2}{E_{221}^2 + 2E_{im}^2 - E_{221} \sqrt{E_{221}^2 + 4E_{210}^2}}. \quad (5.21)$$

It is easy to check that substituting the measured values of the endpoints  $E_{221}$ ,  $E_{210}$  and  $E_{im}$  from (5.9), (5.11) and (5.17), into the three equations above yields the values for the neutrino,  $W$  and top quark mass, correspondingly. Notice that this determination was done in a completely model-independent fashion and without any prior assumptions, unlike the analysis of Ref. [40], which made use the known values of the  $W$  and/or neutrino masses.

Before concluding this section, we should emphasize again that the  $W^+W^-$  and  $t\bar{t}$  data required to test each of the three methods described in this section, already exists at the Tevatron. Therefore we use this opportunity to encourage the CDF and D0 collaborations to perform a model-independent mass determination analysis along the lines presented here.

## 6. Summary and conclusions

In this section we shall briefly summarize our main results.

- We compared the three main methods previously proposed for mass measurements in cascade decays with semi-invisibly decaying particles. We showed that the endpoint method (Sec. 2.1) and the polynomial method (Sec. 2.2) are able to completely determine the mass spectrum only if the decay chain is sufficiently long, namely  $n \geq 3$ . The same conclusion applies if we consider a hybrid combination of the endpoint and polynomial methods. As a corollary, when the decay chain happens to be relatively short,  $n \leq 2$ , these two methods are not sufficient, and one *must* somehow resort to the third,  $M_{T_2}$ , method, in order to completely pin down the mass spectrum. Then in Sec. 2.3 we argued that the  $M_{T_2}$  method *by itself* is sufficient for a complete mass spectrum determination, even in the problematic cases of  $n = 1$  or  $n = 2$ . In Sec. 5 we backed our claim with two explicit examples:  $W^+W^-$  pair production, which is an example of an  $n = 1$  chain, and  $t\bar{t}$  pair production, which is an example of an  $n = 2$  chain. We showed that the  $M_{T_2}$  method in principle provides more than enough measurements for the unambiguous determination of the complete mass spectrum.
- When applying the  $M_{T_2}$  method, we generalized the concept of  $M_{T_2}$  by introducing various subsystem (or subchain)  $M_{T_2}^{(n,p,c)}$  variables. The latter are defined similarly to the conventional  $M_{T_2}$  variable, but are labelled by three integers  $n$ ,  $p$ , and  $c$ , whose meaning is as follows. The integer  $n$  labels the “grandparent” particle originally produced in the hard scattering and initiating the decay chain. We then apply the usual  $M_{T_2}$  concept to the subchain starting at the “parent” particle labelled by  $p$  and terminating at the “child” particle labelled by  $c$ . In general, the “child” particle does not have to be the very last (i.e. the missing) particle in the decay chain, just like the “parent” particle does not have to be the very first particle produced in the event. The introduction of the  $M_{T_2}^{(n,p,c)}$  subchain variables greatly proliferates the number of available  $M_{T_2}$ -type measurements, and allows us to make full use of the power of the  $M_{T_2}$  concept.
- In Sec. 4 and Appendix A we provided analytical expressions for the endpoints of all  $n \leq 2$  subsystem  $M_{T_2}^{(n,p,c)}$  variables, as a function of the corresponding test mass  $\tilde{M}_c$ , and for arbitrary values of the ISR  $p_T$ . Such results for general  $p_T$  are being presented here for the first time. Only some special cases of our results have so far appeared in the literature, for example the functions  $M_{T_2}^{(1,1,0)}(\tilde{M}_0, p_T = 0)$  and  $M_{T_2}^{(2,2,0)}(\tilde{M}_0, p_T = 0)$  were already derived in [32], from where one could also deduce the form of  $M_{T_2}^{(2,2,1)}(\tilde{M}_1, p_T = 0)$ . Our result for  $M_{T_2}^{(2,1,0)}(\tilde{M}_0, p_T = 0)$  discussed in Sec. 4.4 is also new.

- In Sec. 4 we showed that the endpoint functions  $M_{T_2}^{(n,p,c)}(\tilde{M}_c, p_T)$  may exhibit up to three different types of kinks. All three kinks appear in the same location:  $\tilde{M}_c = M_c$ , at which point the value of the subchain endpoint  $M_{T_2, max}^{(n,p,c)}$  coincides with the true parent mass:

$$M_{T_2, max}^{(n,p,c)}(\tilde{M}_c = M_c, p_T) = M_p . \quad (6.1)$$

(This equation generalizes eqs. (4.7), (4.38) and (4.53).) However, the physical origin of each type of kink is different.

1. The first type of kink was originally identified in [30,31] and arises solely as an ISR effect, so that in principle it should always be present at some level. The sharpness of this kink depends on the transverse momentum  $p_T$  of the ISR objects. This particular kink type was responsible for the kink feature  $\Delta\Theta^{(1,1,0)}$  observed in our very first and simplest example in Sec. 4.1. There we generalized the existing analytical formulas for the endpoint  $M_{T_2, max}^{(1,1,0)}$  by including the effects of the ISR. This in turn allowed us to analyze the amount of kink  $\Delta\Theta^{(1,1,0)}$  as a function of the ISR  $p_T$  and the mass spectrum, see Fig. 5.
2. The second type of kink, encountered in Sec. 4.3, was originally discovered in [29,32] and is due to the variable mass of the composite system of visible (SM) particles used in the  $M_{T_2}$  calculation. To be more precise, this type of kink requires the following relation between the parent and child indices:

$$p > c + 1 , \quad (6.2)$$

and does not require any ISR, i.e. it is present even when  $p_T = 0$ . Among the four  $M_{T_2}^{(n,p,c)}$  variables discussed in Sec. 4, only  $M_{T_2}^{(2,2,0)}$  satisfies this condition. Not surprisingly, we encountered this kink during our discussion of the  $M_{T_2, max}^{(2,2,0)}$  endpoint in Sec. 4.3. There we quantified the amount of kink  $\Delta\Theta^{(2,2,0)}$  as a function of the mass spectrum, as shown in Fig. 6(a).

3. The third type of kink, which we encountered in Sec. 4.4 during our discussion of the  $M_{T_2}^{(2,1,0)}$  variable, is new, and to the best of our knowledge has not been discussed in the existing literature<sup>12</sup>. This kink arises due to the decays of heavier particles above the parent level and exists even in the absence of any ISR: its presence simply requires the following relation between the grandparent and parent indices

$$n > p , \quad (6.3)$$

while the child index  $c$  is arbitrary. Because of the upstream objects, this situation does *not* correspond to the balanced momentum configuration discussed

---

<sup>12</sup>Ref. [48] considered the decay chain  $\tilde{q} \rightarrow \tilde{\chi}_2^0 \rightarrow \tilde{\ell} \rightarrow \tilde{\chi}_1^0$  and used the two leptons to form an  $M_{T_2}$  variable which in our notation would correspond to  $M_{T_2}^{(3,2,0)}$ , i.e.  $n = 3$ ,  $p = 2$  and  $c = 0$ . Since this case satisfies both conditions (6.2) and (6.3), the kink observed in [48] is a combination of the second and third kink types according to our classification.

in [28, 32]. Therefore, the analytical expressions for  $M_{T2}$  derived in those two papers are not applicable and will need to be generalized [49]. In general, there are two sources of momentum imbalance in this case: upstream objects from grandparent decays, as well as genuine ISR with  $p_T \neq 0$ . In Sec. 4.4 we concentrated on the former effect and provided analytical expressions for the endpoint function  $M_{T2,max}^{(2,1,0)}(\tilde{M}_0, p_T = 0)$  and the associated kink  $\Delta\Theta^{(2,1,0)}$ , which allowed us to quantify the sharpness of the kink as a function of the mass spectrum, see Fig. 6(b). Comparing Fig. 6(b) to Fig. 6(a), we saw that the new kink  $\Delta\Theta^{(2,1,0)}$  is in general much more pronounced, and therefore offers better prospects for experimental detection. The corresponding formulas for the more general case, when both grandparent decay products and genuine ISR with arbitrary  $p_T$  are present, are listed in Appendix A.

Of course, there are cases when two or even all three of these kinks will be simultaneously present. For example,  $M_{T2,max}^{(2,2,0)}(\tilde{M}_0, p_T \neq 0)$  will exhibit kinks 1 and 2,  $M_{T2,max}^{(2,1,0)}(\tilde{M}_0, p_T \neq 0)$  will exhibit kinks 1 and 3, while  $M_{T2,max}^{(3,2,0)}(\tilde{M}_0, p_T \neq 0)$  will exhibit all three: 1, 2 and 3.

- Our  $M_{T2}$  analysis in Sec. 4 revealed that in the case of an  $n \leq 2$  cascade, there exist 8 different measurements of subsystem  $M_{T2}$  endpoints
  1. One measurement (4.5) of the endpoint  $M_{T2,max}^{(1,1,0)}$  at zero test mass  $\tilde{M}_0$ .
  2. One measurement (4.25) of the endpoint  $M_{T2,max}^{(2,2,1)}$  at zero test mass  $\tilde{M}_1$ .
  3. One measurement (4.43) of the endpoint  $M_{T2,max}^{(2,2,0)}$  at zero test mass  $\tilde{M}_0$ .
  4. Two measurements (4.44) and (4.45) of the endpoint  $M_{T2,max}^{(2,2,0)}$  at two large values ( $E_b$  and  $E'_b$ ) of the test mass  $\tilde{M}_0$ .
  5. One measurement (4.56) of the endpoint  $M_{T2,max}^{(2,1,0)}$  at zero test mass  $\tilde{M}_0$ .
  6. Two measurements (4.57) and (4.58) of the endpoint  $M_{T2,max}^{(2,1,0)}$  at two large values ( $E_b$  and  $E'_b$ ) of the test mass  $\tilde{M}_0$ .

In addition, we also have one measurement of the endpoint (5.16) of the invariant mass distribution  $M_{x_1x_2}$ , bringing the total number of available endpoint measurements to 9. Given that an  $n = 2$  chain contains only three unknown masses  $M_0$ ,  $M_1$  and  $M_2$ , it should be clear that the spectrum can be fully determined. In Sec. 5 we proposed three different methods for mass determinations, depending on what subsets of all those measurements one decides to use. For example, the pure  $M_{T2}$  endpoint method of Sec. 5.1 makes use of different  $M_{T2,max}^{(n,p,c)}(\tilde{M}_c = 0)$  endpoint measurements at zero test mass. The method of Sec. 5.2 makes use of a single  $M_{T2,max}^{(n,p,c)}(\tilde{M}_c)$  function, measured at different values of  $\tilde{M}_c$ . Finally, the hybrid method of Sec. 5.3 combines some of the  $M_{T2,max}^{(n,p,c)}(\tilde{M}_c = 0)$  endpoint measurements at zero test mass with the invariant mass endpoint  $M_{x_1x_2,max}$ .



In conclusion, our work shows that, at least as a matter of principle, the  $M_{T2}$  concept, when properly generalized to include the subsystem variables  $M_{T2}^{(n,p,c)}$ , can allow the measurement of the masses of *all* particles in SUSY-like events with *arbitrary* decay chains at hadron colliders.

## Acknowledgments

We are grateful to A. Barr, B. Gripaios and C. Lester for useful discussions. We dedicate this paper to our parents, grandparents and children. This work is supported in part by a US Department of Energy grant DE-FG02-97ER41029. Fermilab is operated by Fermi Research Alliance, LLC under Contract No. DE-AC02-07CH11359 with the U.S. Department of Energy.

### A. Appendix: Analytical expressions for $M_{T2,max}^{(n,p,c)}(\tilde{M}_c, p_T)$

The purpose of this Appendix is to collect in one place all relevant formulas for the various subsystem  $M_{T2}$  endpoints  $M_{T2,max}^{(n,p,c)}(\tilde{M}_c, p_T)$  in the presence of initial state radiation (ISR) with arbitrary transverse momentum  $p_T$ . In all cases, we will find that  $M_{T2,max}^{(n,p,c)}(\tilde{M}_c, p_T)$  is given by two branches:

$$M_{T2,max}^{(n,p,c)}(\tilde{M}_c, p_T) = \begin{cases} F_L^{(n,p,c)}(\tilde{M}_c, p_T), & \text{if } \tilde{M}_c \leq M_c, \\ F_R^{(n,p,c)}(\tilde{M}_c, p_T), & \text{if } \tilde{M}_c \geq M_c. \end{cases} \quad (\text{A.1})$$

In what follows we shall list the analytic expressions for each branch  $F_L^{(n,p,c)}$  and  $F_R^{(n,p,c)}$ , for all possible  $(n,p,c)$  cases with  $n - c \leq 2$ . The grandparents  $X_n$ , the parents  $X_p$  and the children  $X_c$  are always assumed to be on-shell. However, any intermediate particles  $X_m$  with  $n > m > p$  or  $p > m > c$  may or may not be on-shell, and the two cases will have to be treated differently. Such an example is provided by the endpoint function  $M_{T2,max}^{(n,n,n-2)}(\tilde{M}_{n-2}, p_T)$  discussed below in Section A.2. For convenience, our results will be written in terms of the mass parameters  $\mu_{(n,p,c)}$  defined in (4.1)

$$\mu_{(n,p,c)} \equiv \frac{M_n}{2} \left( 1 - \frac{M_c^2}{M_p^2} \right). \quad (\text{A.2})$$

These parameters represent certain combinations of the masses of the grandparents ( $M_n$ ), parents ( $M_p$ ) and children ( $M_c$ ), and do not contain any dependence on the ISR transverse momentum  $p_T$ . As we discussed in Secs. 4 and 5, these are generally the quantities which are directly measured by experiment. Therefore, with the  $M_{T2}$  method, the goal of any experiment would be to perform a sufficient number of  $\mu$ -parameter measurements and then from those to determine the particle masses themselves.

In some special cases, namely  $n = p$ , we shall also define  $p_T$ -dependent  $\mu$  parameters, where the  $p_T$  dependence is explicitly shown as an argument:

$$\mu_{(n,n,c)}(p_T) = \mu_{(n,n,c)} \left( \sqrt{1 + \left( \frac{p_T}{2M_n} \right)^2} - \frac{p_T}{2M_n} \right). \quad (\text{A.3})$$

When  $p_T = 0$ , the  $p_T$ -dependent parameters (A.3) simply reduce to the  $p_T$ -independent ones (A.2):

$$\mu_{(n,n,c)}(p_T = 0) = \mu_{(n,n,c)}. \quad (\text{A.4})$$

We also remind the reader that test masses for the children are denoted with a tilde:  $\tilde{M}_c$ , while the true mass of any particle does not carry a tilde sign.

### A.1 The subsystem variable $M_{T2,max}^{(n,n,n-1)}(\tilde{M}_{n-1}, p_T)$

The corresponding expressions were already given in eqs. (4.31) and (4.32) and we list them here for completeness:

$$\begin{aligned} F_L^{(n,n,n-1)}(\tilde{M}_{n-1}, p_T) &= \\ &= \left\{ \left[ \mu_{(n,n,n-1)}(p_T) + \sqrt{\left( \mu_{(n,n,n-1)}(p_T) + \frac{p_T}{2} \right)^2 + \tilde{M}_{n-1}^2} \right]^2 - \frac{p_T^2}{4} \right\}^{\frac{1}{2}}, \end{aligned} \quad (\text{A.5})$$

$$\begin{aligned} F_R^{(n,n,n-1)}(\tilde{M}_{n-1}, p_T) &= \\ &= \left\{ \left[ \mu_{(n,n,n-1)}(-p_T) + \sqrt{\left( \mu_{(n,n,n-1)}(-p_T) - \frac{p_T}{2} \right)^2 + \tilde{M}_{n-1}^2} \right]^2 - \frac{p_T^2}{4} \right\}^{\frac{1}{2}}, \end{aligned} \quad (\text{A.6})$$

where the  $p_T$ -dependent parameter  $\mu_{(n,n,n-1)}(p_T)$  was already defined in (A.3):

$$\mu_{(n,n,n-1)}(p_T) = \mu_{(n,n,n-1)} \left( \sqrt{1 + \left( \frac{p_T}{2M_n} \right)^2} - \frac{p_T}{2M_n} \right). \quad (\text{A.7})$$

As already mentioned in Sec. 4.1, the left branch  $F_L^{(n,n,n-1)}$  corresponds to the momentum configuration  $(\vec{p}_{nT}^{(1)} \uparrow \uparrow \vec{p}_{nT}^{(2)}) \uparrow \uparrow \vec{p}_T$ , while the right branch  $F_R^{(n,n,n-1)}$  corresponds to  $(\vec{p}_{nT}^{(1)} \uparrow \uparrow \vec{p}_{nT}^{(2)}) \uparrow \downarrow \vec{p}_T$ .

### A.2 The subsystem variable $M_{T2,max}^{(n,n,n-2)}(\tilde{M}_{n-2}, p_T)$

In this case there is an intermediate particle  $X_{n-1}$  between the parent  $X_n$  and the child  $X_{n-2}$  (see Figs. 1 and 3). Our formulas below are written in such a way that they can be applied both in the case when the intermediate particle  $X_{n-1}$  is on shell ( $M_n > M_{n-1}$ ) and in the case when  $X_{n-1}$  is off-shell ( $M_{n-1} \geq M_n$ ).

In both cases (off-shell or on-shell) we find that the left branch of  $M_{T2,max}^{(n,n,n-2)}(\tilde{M}_{n-2}, p_T)$  is given by

$$F_L^{(n,n,n-2)}(\tilde{M}_{n-2}, p_T) = \left\{ \left[ \mu_{(n,n,n-2)}(p_T) + \sqrt{\left( \mu_{(n,n,n-2)}(p_T) + \frac{p_T}{2} \right)^2 + \tilde{M}_{n-2}^2} \right]^2 - \frac{p_T^2}{4} \right\}^{\frac{1}{2}}, \quad (\text{A.8})$$

where the  $p_T$ -dependent parameter  $\mu_{(n,n,n-2)}(p_T)$  was already defined in (A.3):

$$\mu_{(n,n,n-2)}(p_T) = \mu_{(n,n,n-2)} \left( \sqrt{1 + \left( \frac{p_T}{2M_n} \right)^2} - \frac{p_T}{2M_n} \right). \quad (\text{A.9})$$

The right branch  $F_R^{(n,n,n-2)}$  is given by three different expressions, depending on the mass spectrum and the size of the ISR  $p_T$ :

$$F_R^{(n,n,n-2)}(\tilde{M}_{n-2}, p_T) = \quad (\text{A.10})$$

$$= \begin{cases} F_L^{(n,n,n-2)}(\tilde{M}_{n-2}, -p_T), & \text{if } p_T > \frac{M_n^2 - M_{n-2}^2}{M_{n-2}}, \\ F_{R,off}^{(n,n,n-2)}(\tilde{M}_{n-2}, p_T), & \text{if } p_T \leq \frac{M_n^2 - M_{n-2}^2}{M_{n-2}} \text{ and } \Delta M_{n,n-2}(p_T) \leq M_{x_{n-1}x_n,max}, \\ F_{R,on}^{(n,n,n-2)}(\tilde{M}_{n-2}, p_T), & \text{if } p_T \leq \frac{M_n^2 - M_{n-2}^2}{M_{n-2}} \text{ and } \Delta M_{n,n-2}(p_T) \geq M_{x_{n-1}x_n,max}. \end{cases}$$

Here  $\Delta M_{n,n-2}(p_T)$  is a  $p_T$ -dependent mass parameter defined as

$$\Delta M_{n,n-2}(p_T) \equiv \left\{ \left[ \sqrt{M_n^2 + \frac{p_T^2}{4}} - M_{n-2} \right]^2 - \frac{p_T^2}{4} \right\}^{\frac{1}{2}}, \quad (\text{A.11})$$

which in the limit  $p_T \rightarrow 0$  reduces to

$$\Delta M_{n,n-2}(p_T = 0) = M_n - M_{n-2}, \quad (\text{A.12})$$

justifying its notation. Notice that  $\Delta M_{n,n-2}(p_T)$  is always well-defined, since it is only used when the condition  $p_T \leq (M_n^2 - M_{n-2}^2)/M_{n-2}$  is satisfied and the expression under the square root in (A.11) is nonnegative. The other mass parameter appearing in (A.10),  $M_{x_{n-1}x_n,max}$ , is the familiar endpoint of the invariant mass distribution of the  $\{x_{n-1}, x_n\}$  SM particle pair:

$$M_{x_{n-1}x_n,max} \equiv \begin{cases} \frac{1}{M_{n-1}} \sqrt{(M_n^2 - M_{n-1}^2)(M_{n-1}^2 - M_{n-2}^2)}, & \text{if } M_{n-1} < M_n, \\ M_n - M_{n-2}, & \text{if } M_{n-1} \geq M_n. \end{cases} \quad (\text{A.13})$$

For example, in the special case of  $n = 2$  and the intermediate particle  $X_1$  on-shell, eq. (A.13) reduces to eq. (5.16). The two expressions  $F_{R,off}^{(n,n,n-2)}$  and  $F_{R,on}^{(n,n,n-2)}$  appearing in (A.10) are given by

$$F_{R,off}^{(n,n,n-2)}(\tilde{M}_{n-2}, p_T) = \left\{ \left[ \tilde{M}_{n-2} + \sqrt{\Delta M_{n,n-2}^2(p_T) + \frac{p_T^2}{4}} \right]^2 - \frac{p_T^2}{4} \right\}^{\frac{1}{2}}, \quad (\text{A.14})$$

$$F_{R,on}^{(n,n,n-2)}(\tilde{M}_{n-2}, p_T) = \left\{ \left[ \sqrt{M_{x_{n-1}x_n,max}^2 + p_{vis}^2(p_T)} + \sqrt{\tilde{M}_{n-2}^2 + \left(p_{vis}(p_T) - \frac{p_T}{2}\right)^2} \right]^2 - \frac{p_T^2}{4} \right\}^{\frac{1}{2}}, \quad (\text{A.15})$$

where  $\Delta M_{n,n-2}(p_T)$  and  $M_{x_{n-1}x_n,max}$  were already defined in (A.11) and (A.13), correspondingly. The subscripts ‘‘off’’ and ‘‘on’’ in eqs. (A.14) and (A.15) can be understood as follows. When the intermediate particle  $X_{n-1}$  is off-shell and  $M_{n-1} \geq M_n$ , from (A.11) and (A.13) we get

$$\Delta M_{n,n-2}^2(p_T) = M_n^2 + M_{n-2}^2 - 2M_n M_{n-2} \sqrt{1 + \frac{p_T^2}{4M_n^2}} \leq (M_n - M_{n-2})^2 = M_{x_{n-1}x_n,max}^2. \quad (\text{A.16})$$

Now returning to the logic of eq. (A.10), we see that in the off-shell case at low  $p_T$  one would always use the expression  $F_{R,off}^{(n,n,n-2)}(\tilde{M}_{n-2}, p_T)$  defined in eq. (A.14), and never its alternative  $F_{R,on}^{(n,n,n-2)}(\tilde{M}_{n-2}, p_T)$  from eq. (A.15). To put it another way, the expression  $F_{R,on}^{(n,n,n-2)}(\tilde{M}_{n-2}, p_T)$  in eq. (A.15) is only relevant when the intermediate particle  $X_{n-1}$  is on-shell.

Finally, the quantity  $p_{vis}(p_T)$  appearing in eq. (A.15) is a shorthand notation for the total transverse momentum of the visible particles  $x_n$  and  $x_{n-1}$  in each leg:

$$p_{vis} \equiv |\vec{p}_{nT}^{(k)} + \vec{p}_{(n-1)T}^{(k)}|.$$

In the case relevant for  $F_{R,on}^{(n,n,n-2)}$ , the value of  $p_{vis}$  is given by

$$p_{vis}(p_T) \equiv (\mu_{(n,n,n-1)} + \mu_{(n,n-1,n-2)}) \frac{p_T}{2M_n} + |\mu_{(n,n,n-1)} - \mu_{(n,n-1,n-2)}| \sqrt{1 + \frac{p_T^2}{4M_n^2}}. \quad (\text{A.17})$$

It is easy to check that in the limit of  $p_T \rightarrow 0$  our eqs. (A.8) and (A.10) reduce to the known results for the case of no ISR (eqs. (70) and (74) in Ref. [32]).

The left branch  $F_L^{(n,n,n-2)}$  in (A.8) corresponds to the momentum configuration

$$\left( \vec{p}_{nT}^{(k)} + \vec{p}_{(n-1)T}^{(k)} \right) \uparrow\uparrow \vec{p}_T,$$

while the right branch  $F_R^{(n,n,n-2)}$  in (A.10) corresponds to

$$\left( \vec{p}_{nT}^{(k)} + \vec{p}_{(n-1)T}^{(k)} \right) \uparrow\downarrow \vec{p}_T.$$

In the latter case,  $F_{R,off}^{(n,n,n-2)}$  is obtained when  $X_{n-2}$  is at rest:  $P_{(n-2)T}^{(k)} = 0$ , while  $F_{R,on}^{(n,n,n-2)}$  corresponds to the case when  $P_{(n-2)T}^{(k)} = \frac{1}{2}p_T - p_{vis}(p_T)$ .

### A.3 The subsystem variable $M_{T2,max}^{(n,n-1,n-2)}(\tilde{M}_{n-2}, p_T)$

Here we generalize our  $p_T = 0$  result (4.49) from Sec. 4.4 to the case of arbitrary ISR  $p_T$ :

$$F_L^{(n,n-1,n-2)}(\tilde{M}_{n-2}, p_T) =$$

$$= \left\{ \left[ \mu_{(n-1,n-1,n-2)}(\hat{p}_T) + \sqrt{\left( \mu_{(n-1,n-1,n-2)}(\hat{p}_T) + \frac{\hat{p}_T}{2} \right)^2 + \tilde{M}_{n-2}^2} \right]^2 - \frac{\hat{p}_T^2}{4} \right\}^{\frac{1}{2}}, \quad (\text{A.18})$$

$$F_R^{(n,n-1,n-2)}(\tilde{M}_{n-2}, p_T) =$$

$$= \left\{ \left[ \mu_{(n-1,n-1,n-2)}(-\hat{p}_T) + \sqrt{\left( \mu_{(n-1,n-1,n-2)}(-\hat{p}_T) - \frac{\hat{p}_T}{2} \right)^2 + \tilde{M}_{n-2}^2} \right]^2 - \frac{\hat{p}_T^2}{4} \right\}^{\frac{1}{2}} \quad (\text{A.19})$$

where we have introduced the shorthand notation

$$\hat{p}_T \equiv p_T + 2\mu_{(n,n,n-1)}(p_T). \quad (\text{A.20})$$

Notice that the second term on the right-hand side contains the  $p_T$ -dependent  $\mu$  parameter defined in (A.7).

The left branch  $F_L^{(n,n-1,n-2)}$  in (A.18) corresponds to the momentum configuration

$$\vec{p}_{(n-1)T}^{(k)} \uparrow\uparrow \left( \vec{p}_{nT}^{(k)} \uparrow\uparrow \vec{p}_T \right),$$

while the right branch  $F_R^{(n,n-1,n-2)}$  in (A.19) corresponds to

$$\vec{p}_{(n-1)T}^{(k)} \uparrow\downarrow \left( \vec{p}_{nT}^{(k)} \uparrow\uparrow \vec{p}_T \right).$$

It is worth checking that our general  $p_T$ -dependent results (A.18) and (A.19) reduce to our previous formulas (4.50) and (4.51) in the  $p_T \rightarrow 0$  limit and in the special case of  $n = 2$ . First taking the limit  $p_T \rightarrow 0$  from (A.20) and (A.7) we get

$$\lim_{p_T \rightarrow 0} \hat{p}_T = 2\mu_{(n,n,n-1)}, \quad (\text{A.21})$$

$$\lim_{p_T \rightarrow 0} \mu_{(n-1,n-1,n-2)}(\hat{p}_T) = \mu_{(n-1,n-1,n-2)}(2\mu_{(n,n,n-1)}) = \mu_{(n,n,n-2)} - \mu_{(n,n,n-1)}, \quad (\text{A.22})$$

$$\lim_{p_T \rightarrow 0} \mu_{(n-1,n-1,n-2)}(-\hat{p}_T) = \mu_{(n-1,n-1,n-2)}(-2\mu_{(n,n,n-1)}) = \mu_{(n,n-1,n-2)}. \quad (\text{A.23})$$

Substituting (A.21-A.23) into (A.18) and (A.19), we get

$$\begin{aligned} & F_L^{(n,n-1,n-2)}(\tilde{M}_{n-2}, p_T = 0) = \\ & = \left\{ \left[ \mu_{(n,n,n-2)} - \mu_{(n,n,n-1)} + \sqrt{\mu_{(n,n,n-2)}^2 + \tilde{M}_{n-2}^2} \right]^2 - \mu_{(n,n,n-1)}^2 \right\}^{\frac{1}{2}}, \end{aligned} \quad (\text{A.24})$$

$$\begin{aligned} & F_R^{(n,n-1,n-2)}(\tilde{M}_{n-2}, p_T = 0) = \\ & = \left\{ \left[ \mu_{(n,n-1,n-2)} + \sqrt{(\mu_{(n,n,n-1)} - \mu_{(n,n-1,n-2)})^2 + \tilde{M}_{n-2}^2} \right]^2 - \mu_{(n,n,n-1)}^2 \right\}^{\frac{1}{2}}, \end{aligned} \quad (\text{A.25})$$

which are nothing but the generalizations of (4.50) and (4.51) for arbitrary  $n$ .

## References

- [1] G. Bertone, D. Hooper and J. Silk, “Particle dark matter: Evidence, candidates and constraints,” *Phys. Rept.* **405**, 279 (2005) [arXiv:hep-ph/0404175].
- [2] See, for example, J. Hubisz, J. Lykken, M. Pierini and M. Spiropulu, “Missing energy look-alikes with 100 pb-1 at the LHC,” arXiv:0805.2398 [hep-ph], and references therein.
- [3] G. Jungman, M. Kamionkowski and K. Griest, “Supersymmetric dark matter,” *Phys. Rept.* **267**, 195 (1996) [arXiv:hep-ph/9506380].
- [4] T. Appelquist, H. C. Cheng and B. A. Dobrescu, “Bounds on universal extra dimensions,” *Phys. Rev. D* **64**, 035002 (2001) [arXiv:hep-ph/0012100].
- [5] H. C. Cheng, K. T. Matchev and M. Schmaltz, “Bosonic supersymmetry? Getting fooled at the LHC,” *Phys. Rev. D* **66**, 056006 (2002) [arXiv:hep-ph/0205314].
- [6] K. Agashe, A. Falkowski, I. Low and G. Servant, “KK Parity in Warped Extra Dimension,” *JHEP* **0804**, 027 (2008) [arXiv:0712.2455 [hep-ph]].
- [7] S. Arrenberg, L. Baudis, K. Kong, K. T. Matchev and J. Yoo, “Kaluza-Klein Dark Matter: Direct Detection vis-a-vis LHC,” arXiv:0805.4210 [hep-ph].
- [8] H. C. Cheng and I. Low, “TeV symmetry and the little hierarchy problem,” *JHEP* **0309**, 051 (2003) [arXiv:hep-ph/0308199].
- [9] A. Birkedal, A. Noble, M. Perelstein and A. Spray, “Little Higgs dark matter,” *Phys. Rev. D* **74**, 035002 (2006) [arXiv:hep-ph/0603077].
- [10] T. Hur, H. S. Lee and S. Nasri, “A Supersymmetric U(1)’ Model with Multiple Dark Matters,” *Phys. Rev. D* **77**, 015008 (2008) [arXiv:0710.2653 [hep-ph]].
- [11] H. S. Lee, “Lightest U-parity Particle (LUP) dark matter,” *Phys. Lett. B* **663**, 255 (2008) [arXiv:0802.0506 [hep-ph]].
- [12] I. Hinchliffe, F. E. Paige, M. D. Shapiro, J. Soderqvist and W. Yao, “Precision SUSY measurements at LHC,” *Phys. Rev. D* **55**, 5520 (1997) [arXiv:hep-ph/9610544].
- [13] C. G. Lester and D. J. Summers, “Measuring masses of semi-invisibly decaying particles pair produced at hadron colliders,” *Phys. Lett. B* **463**, 99 (1999) [arXiv:hep-ph/9906349].
- [14] H. Bachacou, I. Hinchliffe and F. E. Paige, “Measurements of masses in SUGRA models at LHC,” *Phys. Rev. D* **62**, 015009 (2000) [arXiv:hep-ph/9907518].
- [15] I. Hinchliffe and F. E. Paige, “Measurements in SUGRA models with large tan(beta) at LHC,” *Phys. Rev. D* **61**, 095011 (2000) [arXiv:hep-ph/9907519].
- [16] B. C. Allanach, C. G. Lester, M. A. Parker and B. R. Webber, “Measuring sparticle masses in non-universal string inspired models at the LHC,” *JHEP* **0009**, 004 (2000) [arXiv:hep-ph/0007009].
- [17] A. Barr, C. Lester and P. Stephens, “m(T2): The truth behind the glamour,” *J. Phys. G* **29**, 2343 (2003) [arXiv:hep-ph/0304226].
- [18] M. M. Nojiri, G. Polesello and D. R. Tovey, “Proposal for a new reconstruction technique for SUSY processes at the LHC,” arXiv:hep-ph/0312317.

- [19] K. Kawagoe, M. M. Nojiri and G. Polesello, “A new SUSY mass reconstruction method at the CERN LHC,” *Phys. Rev. D* **71**, 035008 (2005) [arXiv:hep-ph/0410160].
- [20] B. K. Gjelsten, D. J. Miller and P. Osland, “Measurement of SUSY masses via cascade decays for SPS 1a,” *JHEP* **0412**, 003 (2004) [arXiv:hep-ph/0410303].
- [21] B. K. Gjelsten, D. J. Miller and P. Osland, “Measurement of the gluino mass via cascade decays for SPS 1a,” *JHEP* **0506**, 015 (2005) [arXiv:hep-ph/0501033].
- [22] A. Birkedal, R. C. Group and K. Matchev, “Slepton mass measurements at the LHC,” *In the Proceedings of 2005 International Linear Collider Workshop (LCWS 2005), Stanford, California, 18-22 Mar 2005, pp 0210* [arXiv:hep-ph/0507002].
- [23] D. J. Miller, P. Osland and A. R. Raklev, “Invariant mass distributions in cascade decays,” *JHEP* **0603**, 034 (2006) [arXiv:hep-ph/0510356].
- [24] P. Meade and M. Reece, “Top partners at the LHC: Spin and mass measurement,” *Phys. Rev. D* **74**, 015010 (2006) [arXiv:hep-ph/0601124].
- [25] B. K. Gjelsten, D. J. Miller, P. Osland and A. R. Raklev, “Mass determination in cascade decays using shape formulas,” *AIP Conf. Proc.* **903**, 257 (2007) [arXiv:hep-ph/0611259].
- [26] S. Matsumoto, M. M. Nojiri and D. Nomura, “Hunting for the top partner in the littlest Higgs model with T-parity at the LHC,” *Phys. Rev. D* **75**, 055006 (2007) [arXiv:hep-ph/0612249].
- [27] H. C. Cheng, J. F. Gunion, Z. Han, G. Marandella and B. McElrath, “Mass Determination in SUSY-like Events with Missing Energy,” *JHEP* **0712**, 076 (2007) [arXiv:0707.0030 [hep-ph]].
- [28] C. Lester and A. Barr, “MTGEN : Mass scale measurements in pair-production at colliders,” *JHEP* **0712**, 102 (2007) [arXiv:0708.1028 [hep-ph]].
- [29] W. S. Cho, K. Choi, Y. G. Kim and C. B. Park, “Gluino Stransverse Mass,” *Phys. Rev. Lett.* **100**, 171801 (2008) [arXiv:0709.0288 [hep-ph]].
- [30] B. Gripaios, “Transverse Observables and Mass Determination at Hadron Colliders,” *JHEP* **0802**, 053 (2008) [arXiv:0709.2740 [hep-ph]].
- [31] A. J. Barr, B. Gripaios and C. G. Lester, “Weighing Wimps with Kinks at Colliders: Invisible Particle Mass Measurements from Endpoints,” *JHEP* **0802**, 014 (2008) [arXiv:0711.4008 [hep-ph]].
- [32] W. S. Cho, K. Choi, Y. G. Kim and C. B. Park, “Measuring superparticle masses at hadron collider using the transverse mass kink,” *JHEP* **0802**, 035 (2008) [arXiv:0711.4526 [hep-ph]].
- [33] G. G. Ross and M. Serna, “Mass Determination of New States at Hadron Colliders,” *Phys. Lett. B* **665**, 212 (2008) [arXiv:0712.0943 [hep-ph]].
- [34] M. M. Nojiri, G. Polesello and D. R. Tovey, “A hybrid method for determining SUSY particle masses at the LHC with fully identified cascade decays,” *JHEP* **0805**, 014 (2008) [arXiv:0712.2718 [hep-ph]].
- [35] P. Huang, N. Kersting and H. H. Yang, “Hidden Thresholds: A Technique for Reconstructing New Physics Masses at Hadron Colliders,” arXiv:0802.0022 [hep-ph].
- [36] M. M. Nojiri, Y. Shimizu, S. Okada and K. Kawagoe, “Inclusive transverse mass analysis for squark and gluino mass determination,” *JHEP* **0806**, 035 (2008) [arXiv:0802.2412 [hep-ph]].

- [37] D. R. Tovey, “On measuring the masses of pair-produced semi-invisibly decaying particles at hadron colliders,” *JHEP* **0804**, 034 (2008) [arXiv:0802.2879 [hep-ph]].
- [38] M. M. Nojiri and M. Takeuchi, “Study of the top reconstruction in top-partner events at the LHC,” arXiv:0802.4142 [hep-ph].
- [39] H. C. Cheng, D. Engelhardt, J. F. Gunion, Z. Han and B. McElrath, “Accurate Mass Determinations in Decay Chains with Missing Energy,” *Phys. Rev. Lett.* **100**, 252001 (2008) [arXiv:0802.4290 [hep-ph]].
- [40] W. S. Cho, K. Choi, Y. G. Kim and C. B. Park, “Measuring the top quark mass with  $m_{T2}$  at the LHC,” *Phys. Rev. D* **78**, 034019 (2008) [arXiv:0804.2185 [hep-ph]].
- [41] M. Serna, “A short comparison between  $m_{T2}$  and  $m_{CT}$ ,” *JHEP* **0806**, 004 (2008) [arXiv:0804.3344 [hep-ph]].
- [42] M. Bisset, R. Lu and N. Kersting, “Improving SUSY Spectrum Determinations at the LHC with Wedgebox and Hidden Threshold Techniques,” arXiv:0806.2492 [hep-ph].
- [43] A. J. Barr, G. G. Ross and M. Serna, “The Precision Determination of Invisible-Particle Masses at the LHC,” arXiv:0806.3224 [hep-ph].
- [44] N. Kersting, “On Measuring Split-SUSY Gaugino Masses at the LHC,” arXiv:0806.4238 [hep-ph].
- [45] M. M. Nojiri, K. Sakurai, Y. Shimizu and M. Takeuchi, “Handling jets + missing  $E_T$  channel using inclusive  $m_{T2}$ ,” arXiv:0808.1094 [hep-ph].
- [46] M. Burns, K. Kong, K. T. Matchev and M. Park, “A General Method for Model-Independent Measurements of Particle Spins, Couplings and Mixing Angles in Cascade Decays with Missing Energy at Hadron Colliders,” *JHEP* **0810**, 081 (2008), arXiv:0808.2472 [hep-ph].
- [47] W. S. Cho, K. Choi, Y. G. Kim and C. B. Park, “ $M_{T2}$ -assisted on-shell reconstruction of missing momenta and its application to spin measurement at the LHC,” arXiv:0810.4853 [hep-ph].
- [48] H. C. Cheng and Z. Han, “Minimal Kinematic Constraints and  $MT2$ ,” arXiv:0810.5178 [hep-ph].
- [49] M. Burns, K. Kong, K. Matchev and M. Park, in preparation.
- [50] B. K. Gjelsten, D. J. Miller, P. Osland and A. R. Raklev, “Mass ambiguities in cascade decays,” arXiv:hep-ph/0611080.
- [51] M. Park, talk at Pheno 2008.
- [52] G. Weiglein *et al.* [LHC/LC Study Group], “Physics interplay of the LHC and the ILC,” *Phys. Rept.* **426**, 47 (2006) [arXiv:hep-ph/0410364].